BIOELECTRONIC SYSTEMS IN STUDYING TISSUE ENGINEERING, REAL-TIME BIOPHYSICAL MONITORING OF BIRDS AND POINT-OF-CARE DIAGNOSTICS

A Dissertation

Presented to the Faculty of the Graduate School

of Cornell University

in Partial Fulfillment of the Requirements for the Degree of

Doctor of Philosophy

by

Abdurrahman Gumus

January 2015

BIOELECTRONIC SYSTEMS IN STUDYING TISSUE ENGINEERING, REAL-TIME BIOPHYSICAL MONITORING OF BIRDS AND POINT-OF-CARE DIAGNOSTICS

Abdurrahman Gumus, Ph.D.

Cornell University 2015

The field of bioelectronics started about 18th century with the frog experiments of Luigi Galvani by moving the detached leg of frog with the application of a small voltage. Today there are variety of bioelectronic devices available in many different areas such as pacemakers, continuous glucose sensors, implantable brain tissue interfaces, that show how far we have gone since the Galvani experiments. This dissertation introduces bioelectronic systems for different research areas such as tissue engineering, biophysical monitoring of birds and point-of-care diagnostics.

First, we have introduced a device depends on organic bioelectronics, a growing research field that integrates organic electronic materials with biological systems, and used it for tissue engineering purposes. We have developed a planar device that contains a conducting polymer stripe and achieves a continuum of microenvironments for cell growth under the influence of an applied bias. Marked differences are observed in the migration behaviors of bovine aortic endothelial cells (EC) as a function of location along the polymer stripe, and 3-fold variation is achieved in EC migration

speed and directional persistence time. A gradient in adsorbed fibronectin indicates that a spatial variation in cell adhesion is at play. We have used our device to modulate the cell adhesion and changed cell density gradients of normal and cancerous cell lines by inducing electrically which can be used as a tool for the study of cell-cell interactions.

Next, we have developed a real-time *in vivo* uric acid biosensor system, Lab-on-a-Bird, for biophysical monitoring of birds. The metabolism of birds is finely tuned to their activities and environments, and thus research on avian systems can play an important role in understanding organismal responses to environmental changes and ecological investigations. After characterization of the sensor system, we demonstrated the autonomous operation of the system by collecting *in vivo* extracellular uric acid measurements on a domestic chicken. We then show how the device can be used to monitor, in real time, the effects of short-term flight and rest cycles on the uric acid levels of pigeons. In addition, we demonstrate that our device has the ability to measure uric acid level increase in homing pigeons while they fly freely to back home. Successful application of the sensor in migratory birds could open up a new way of studying birds in flight which would lead to a better understanding of the ecology and biology of avian movements.

Finally, we have presented a Cholera-Detect system for point-of-care detection of *Vibrio Cholerae* which is a comma-shaped, gram negative bacterium and the cause of an acute diarrhoeal disease in humans called “Cholera”. Even though up to 80% of

the cases can be successfully treated with oral rehydration salts, around 100,000 – 120,000 of the cases come to an end as deaths. This indicates that early and rapid detection of the cholera is necessary to prevent spread of disease, increase the efficiency of treatments and decrease the intensity of epidemics. Cholera-Detect system has the ability to do rapid, and on-field molecular diagnosis of cholera without need for extensive laboratory equipment and chemicals which would potentially make possible improved health care in outbreak situations.

BIOGRAPHICAL SKETCH

Abdurrahman Gumus was born and raised in Istanbul, Turkey. He graduated from the Department of Electrical and Electronics Engineering at Istanbul University in 2005 with an honors degree. He continued his masters and doctoral studies at Cornell University, School of Electrical and Computer Engineering, where he developed bioelectronic systems for tissue engineering, real-time biophysical monitoring of birds and point-of-care diagnostics and received his Ph.D. degree in 2015.

Dedicated to

the pursuit of knowledge,

my parents Ayfer and Dursun Gumus,

my bellowed wife Fatma,

and the NOW, which is all that we have..

ACKNOWLEDGEMENTS

I would like to express my heartfelt gratitude to my advisor, Professor David Erickson, for his excellent guidance, support, and encouragement. I appreciate for his confidence in me and giving me the opportunity to conduct research in many different areas. His endless support on my work, useful advices, helpful insights and sincere friendship lie at the heart of my success at Cornell. I have learned a lot from him not just scientifically, but also about being a brilliant advisor. It was my privilege to work with him, and I look forward to future collaborations.

I would like to thank to my previous advisor, Professor George Malliaras, for his guidance and endless support at the first year of my Ph.D. journey. I feel lucky for having the privilege to observe a great mind like him in action. I also would like to thank to Professor Cynthia Reinhart-King for her support and guidance. She was always open to new research ideas and patiently supported and helped me to conduct cool research in her very enthusiastic research group.

I am also indebted my committee: Professor David Winkler, Antje Baeumner, and Rajit Manohar for their suggestions and encouragement. I would like to especially thank to Professor Winkler for his endless support for the Lab-on-a-Bird project. His useful advices and helpful insights helped us to move forward and get exciting results. I would like to thank to Professor Baeumner for his support and suggestions. I feel

myself very lucky to be close to a great scientist like her and have a chance to learn about biosensors from her. I would always remember the excitement that she had in her eyes while teaching in the class.

I have been also fortunate to have a wonderful group of friends at Cornell that includes my lab mates in Erickson Lab and Malliaras Lab, users and staff of CNF and NBTC. Especially to the people of the Erickson Lab, you were like a family to me.

Finally, I would like to thank my parents Ayfer Gumus and Dursun Gumus and bellowed wife Fatma Gumus for their support throughout my studies. Without their support and love, I would not be here today.

TABLE OF CONTENTS

LIST OF FIGURES

CHAPTER 1

INTRODUCTION

1.1 Electronics at the interface with biology

Interfacing electronic devices with biological systems has many application areas in medical diagnostics, healthcare and biomedical engineering. This interaction could be two sided: biological inputs to the electrical systems or electrical inputs to the biological systems (Fig. 1.1). In the case of biological inputs, electronic element converts the biological signals into measurable electrical signals which can then be analyzed for its significance. In the case of electrical inputs (electrodes, transistors, etc.), behavior or function of the biological system can be affected by electrical stimulus.

The development of biological sensing capabilities that have the ability to transduce the biorecognition or biocatalytic process in the form of electronic signals are one of the major activities in the field of bioelectronics. One of the well-known and most widely successful example to date is the blood glucose sensor which is an important commercially available diagnostics tool for diabetic patients throughout the world. By combining continuous glucose monitoring sensor and insulin drug delivery system, an artificial pancreas has been created which has the potential to transform the

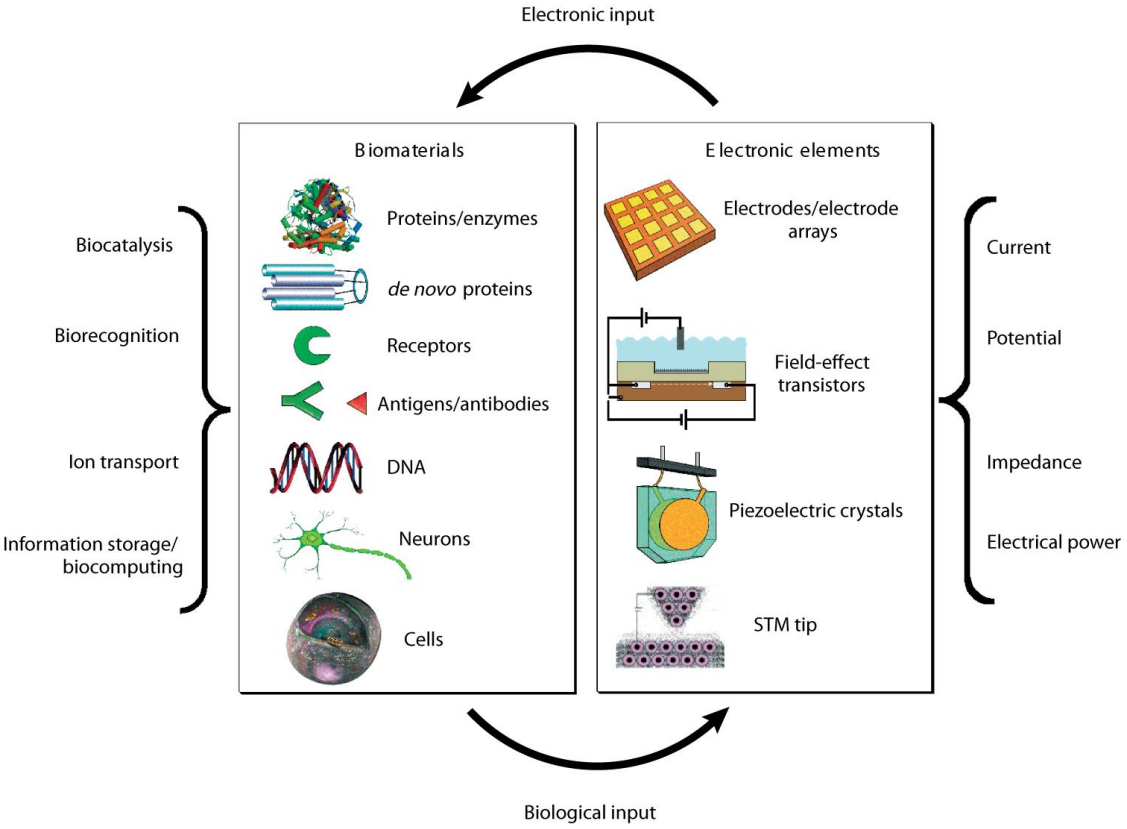

Fig. 1.1: Interaction of biomaterials (left) and electronic systems (right) for bioelectronic applications. Reproduced with permission from *Bioelectronics: From Theory to Applications* [1].

lives of people with type 1 diabetes. Although many other biological sensing platforms have been introduced to the literature with high sensitivity, specificity and parallelity in order to meet the needs of a variety fields ranging from medical diagnostics to pharmaceutical discovery, demand is increasing for innovation by growing aging population and increased chronic diseases.

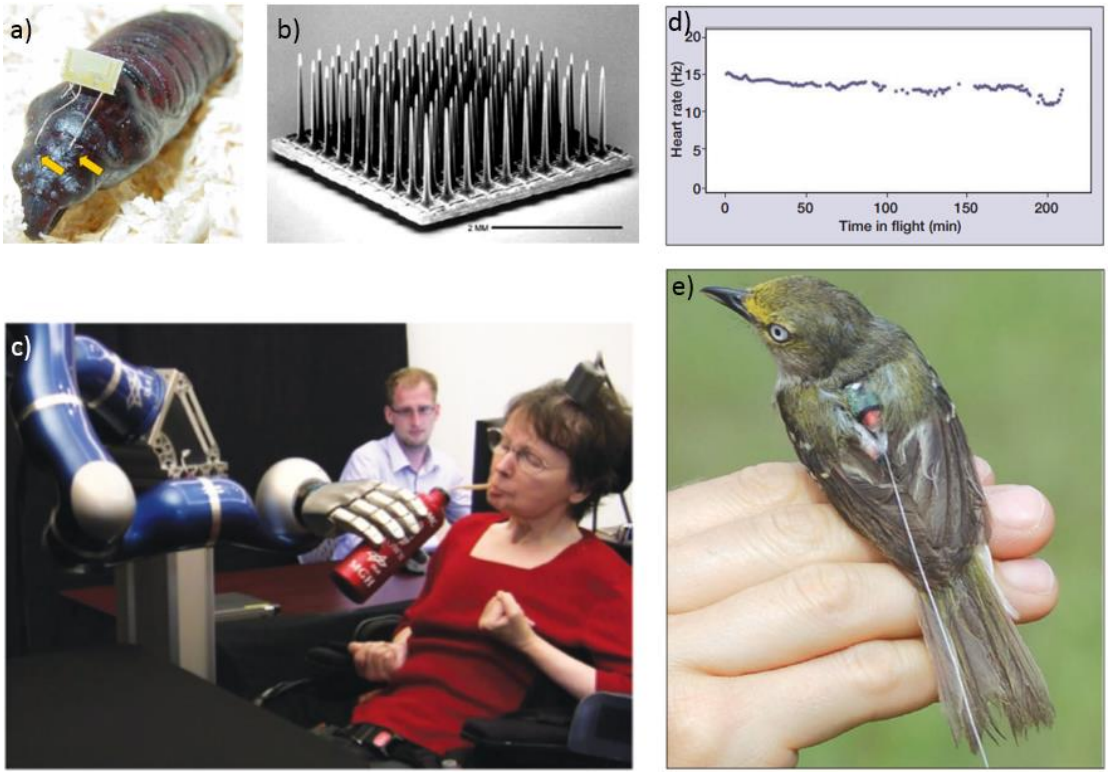

Fig. 1.2: a) Metal microprobes are inserted into the insect brain and thorax tissue at the pupil stage. The probes emerge with the tissue around which gives a mechanically and electrically reliable interface [2]. b) Intracortical silicon microelectrode array. These electrodes penetrate into the brain tissue and record the activity of the brain cells at specific region [4]. c) Translating neural activity of the brain directly into control signals give the ability to control assistive devices [5, 6]. d) Example of physiological measurements from a migrating bird (Swainson's thrush) which shows the heart rate of a free-flying. This helped the researchers to calculate the rate of energy expenditure during the flight [7]. e) A bird (White-eyed vireo) with heart rate monitoring system installed on it [8].

To interface electronics systems with living tissue, the pacemaker is one of the most important and mature therapeutic technologies that stimulate electrically-active

cells of the hart to control abnormal heart rhythms. Cochlear implant is another widely used example of bioelectronic systems which provides a sense of sound to a person who is profoundly deaf or severely hard of hearing. There are other examples of bioelectronic devices that can restore lost function for patients and improve the quality of life such as ocular implants to provide artificial vision and prosthetic limbs that can interface with the human nervous system [4]. There is also ongoing effort for brain tissue interfaces for people with paralysis (Fig. 1.2c). Recording signals from motor cortex neurons using silicon micro-electrode array and translating neural activity directly into control signals for assistive devices give the ability to control a robotic-arm to perform three-dimensional reach and grasp movements, even use a robotic arm to drink a coffee from a bottle [9].

Bioelectronic systems has been also used for animals. Brain machine interface was installed on able-bodied monkeys to move and click the computer cursor or control a robotic arm [5, 6]. Insect-machine interface is another exciting application area of bioelectronics which gives the ability to control navigation of flight in months. Metal microprobes were implanted into the insect brain and thorax tissue using early metamorphosis insertion technology. A possible demonstration of these systems would be environmental monitoring or search and rescue operation at the time of disasters when equipped with appropriate instruments [2, 10, 11]. Technological advances in tracking and sensing devices have also opened new opportunities to study of migratory birds which are mostly physically too small (Fig. 1d and Fig. 1e). This is important

because research on birds can serve as an effective tool for ecological and evolutionary studies, as the metabolism of birds are finely tuned to their environments [12]. Combining sensors with tracking data promises a better way of understanding avian movement and biology.

Smartphones can be also count as bioelectronic systems. Increasing demand and availability of smartphone technology is also another transformative opportunity for the deployment of bioelectronic devices. Imaging, computation and communication capabilities and their interaction with sensors and diagnostic devices would enable to have more informative systems directly to the consumers allowing them to take better control of their own health [3]. Point-of-care (POC) diagnostic devices usually combine a two part system: a consumable chip that detects the analyte of interest, and an instrument type reader, bioelectric component, that interprets the signal from the chip and provides results to the user. Smartphone will be transformative both in developing and developed world for personalized healthcare applications because most consumers will already own a test reader/instrument in the form of a smartphone. Especially lab-on-a-chip diagnostics in resource limited settings will help early-stage diagnosis, better communication with patients and better tracking of disease outbreaks [3]. Smartphones can also be incorporated wearable and implantable body sensors networks for

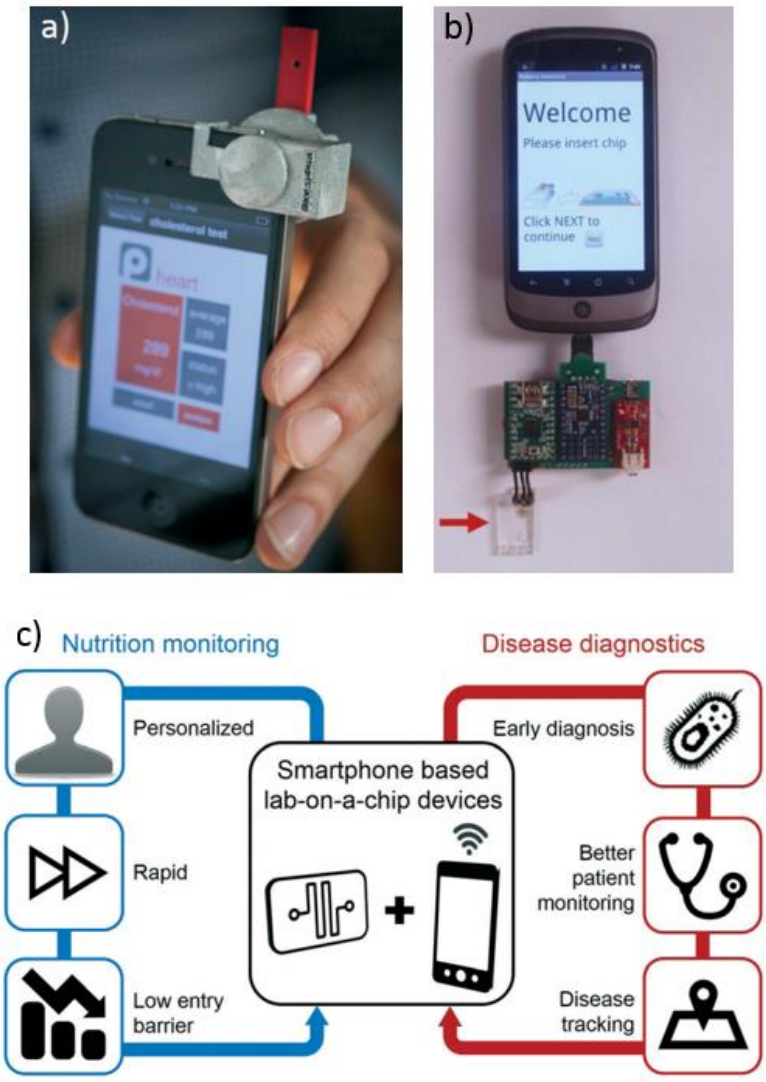

Fig. 1.3: a) Smartphone based colorimetric analysis for serum cholesterol detection and b) electrochemistry analysis. c) Smartphones can be also count as bioelectronic systems and incorporating them with lab-on-a-chip technologies, wearable and implantable sensors will be transformative for healthcare applications and early diagnosis and tracking of diseases [3].

continuous monitoring of patients and minimize the need for caregivers, help the chronically ill and elderly people live an independent life and early detection of

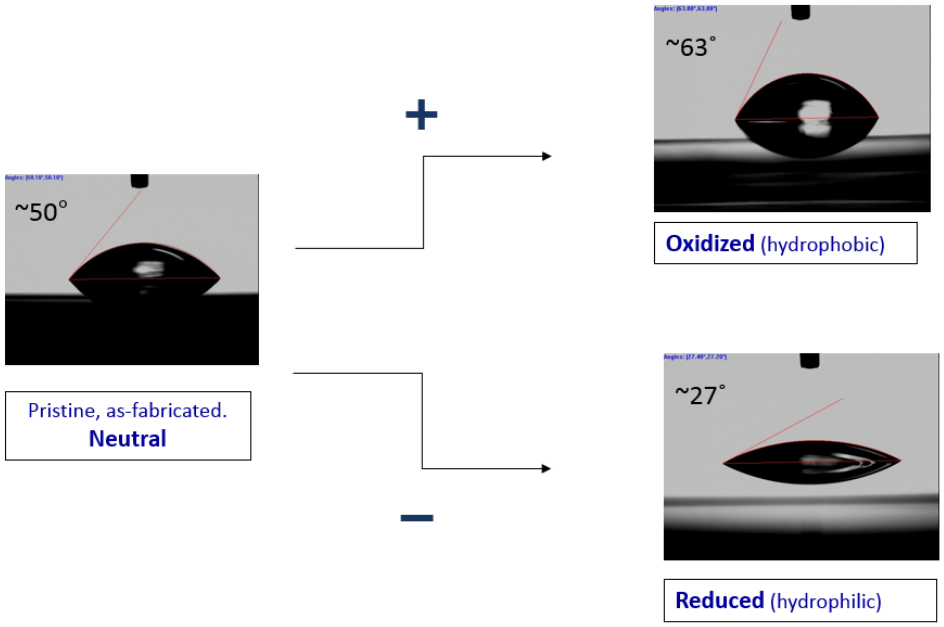

Fig. 1.4: Water contact angle measurements on oxidized and reduced conducting polymer (PEDOT:Tosylate) surfaces which shows the tunability of surface energy/hydrophilicity.

emergency conditions [13].

The use of organic electronic materials in bioelectronic applications also offers many opportunities and is fueled by some unique features of these materials such as the ability to transport ions, similar mechanical properties to those of tissue, their ease and low cost of processing, their compatibility with flexible substrates and low temperature processing [14]. Because of the soft nature and flexibility of the organic materials, they have better mechanical compatibility with tissues rather than traditional electronic materials. Organic materials allow for oxide free interfaces when they are in contact with aqueous electrolytes and therefore they can be in direct contact with the

biological environments such cell cultures or tissue implants. One of the most important properties of organic materials is the tunability of their properties through doping. When ions from an electrolyte enter an organic film, or vice versa, a change in the doping state occurs. This gives the ability to organics to conduct ions in addition to electrons and holes which opens up a new communication channel with biology. The doping can be achieved through "electrochemical doping" where a metal gate electrode immersed into the electrolyte and positive charge is supplied through it, then cations from the electrolyte enter the conducting polymer film and compensate the anions, thereby decreasing the hole density on conducting polymer. This reversible process makes organic materials ideal electron-to-ion converters which is a key property for communicating between the electronics and biology. On the other hand, many properties of organic electronic materials can be changed by electrochemical doping/de-doing process such as surface energy (hydrophilicity/hydrophobicity) (Fig. 1.4), surface charge, stiffness and chemistry which make them ideal tool for studies where active interaction with living cell and tissues are necessary [15-19].

While many successful applications of bioelectronic devices and systems exist, much work may remain to be done at the interface between electronics and living systems. By combining research efforts of biologists, chemists, physicists, materials scientists and electronic engineers, and also having close collaboration of industry, academia and the medical community, bioelectronics promise a bright future for

impressive advances that enable us to better understand and manipulate the biological systems, improve healthcare and quality of life.

1.2 Organization of the Dissertation

Through the dissertation, we wanted to find answers to some of the important questions of bioelectronic systems in tissue engineering, real-time biophysical monitoring of birds and POC diagnostic applications. In the first part of the thesis, Chapter 2 and 3, we have investigated a conducting polymer device as an "active" substrate for cell culturing and the effect of redox state change on the cell behavior such as cell migration and adhesion. In Chapter 4 and 5, real-time *in vivo* uric acid biosensor system was introduced and its demonstrations on physiological monitoring in domestic chicken and flying pigeons were investigated. In Chapter 6, we have developed a system that exploits the solar thermal energy to simple nucleic acid extraction and isolation, polymerase chain reaction (PCR) based amplification, and smartphone assisted analysis of the results.

CHAPTER 2

ELECTRICAL CONTROL OF CELL MIGRATION USING A CONDUCTING POLYMER DEVICE

2.1 Abstract

Control of cell migration is receiving a great deal of attention due to its relevance to the engineering of tissues. Here we report a device that contains a conducting polymer stripe and achieves a continuum of microenvironments for cell growth under the influence of an applied bias. Marked differences are observed in the migration behaviour of bovine aortic endothelial cells (ECs) as a function of location along the polymer stripe, and a 3-fold variation is achieved in EC migration speed and directional persistence time. Moreover, the device induces directional cell migration along the conducting polymer stripe. A gradient in adsorbed fibronectin indicates that a spatial variation in cell adhesion is at play. The ability to control cell migration behaviour using external electrical stimuli highlights the potential of using conducting polymers as ‘‘active’’ substrates for the non-invasive control of cell behaviour.

This work was published in *Soft Matter* in 2010 [14]. All figures reproduced with permission.

2.2 Introduction

The directed assembly of cells into tissues is critical to embryonic development, wound healing and the engineering of tissues for organ regeneration and replacement [20]. Cell migration, which facilitates proper spatial localization during tissue formation, is largely controlled by the chemical and structural cues in the microenvironment that are integrated by the molecular machinery of cells. As a result, the engineering of well-defined extracellular matrix environments that control cell migration by altering the chemical, mechanical or structural properties of the extracellular scaffold [21] is receiving a great deal of attention.

Tissue engineering largely focuses on developing materials that induce physiological cell migration and tissue assembly by incorporating the extracellular cues found in vivo. It is wellestablished that soluble and insoluble chemical gradients [22, 23], gradients in mechanical stiffness [24, 25] and micro- and nanotopographical features [26] can be exploited to direct and/or enhance cell migration. It is known that cells can respond to chemical gradients of growth factors through chemotaxis and haptotaxis, and gradients in mechanical stiffness through durotaxis. As such, many biomaterials and devices have been engineered by using novel polymers, chemical conjugation techniques or microfluidics to present well-defined chemical or mechanical gradients to cells.

The goal of these platforms has been to induce cell migration as a critical step in forming replacement tissues. Many of the current strategies have limitations. In the case of chemotaxis based approaches, it has been difficult to achieve long-term, stable gradients to induce cell migration on an implantable device. In durotaxis, most materials that have been developed to incorporate tunable, well-defined mechanical gradients are not biocompatible and would not be suitable for implantation. Therefore, there is a clear need to develop better strategies to reliably and easily control cell migration using a method amenable to implantation.

The emergence of organic electronics – a technology that relies on carbon-based semiconductors to deliver devices with unique properties [27] – creates tremendous opportunities at the interface between electronic materials and living cells [14]: The ‘‘soft’’ nature of organics offers better mechanical compatibility with tissue than traditional electronic materials, while their natural compatibility with mechanically flexible substrates suits the non-planar forms often required for biomedical implants [28]. Their ability to conduct both ionic and electronic charges opens up a new communication channel with electrically active cells [29, 30]. Finally, the fact that the electronic properties of organics can be altered in response to electrical stimuli [31] creates opportunities to use these materials as ‘‘active’’ substrates for cell growth.

In 1994, Wong *et al.* discovered that ECs grow differently on oxidized versus reduced polypyrrole films [32]. Since conducting polymers such as polypyrrole can be

reversibly switched between oxidized and reduced states, these experiments paved the way for non-invasive control of cell behaviour by electrical means. More recently, devices based on a conducting polythiophene have been used to demonstrate electrical control of cell adhesion [33], and the creation of density gradients in normal and cancerous cell lines [17].

In this study, we take a look at the influence of the redox state of a conducting polymer on the migration of individual cells. We demonstrate that organic electronic devices enable the electrical control of cell migration, hence they can serve as vehicles to help understand and engineer tissue formation.

2.3 Results and Discussion

A device that allows one to create a continuum of microenvironments for cell growth is shown in Fig. 1. An indium tin oxide (ITO) stripe was deposited on a glass substrate, onto which a polydimethylsiloxane (PDMS) reservoir containing cell growth medium was attached. A ground electrode was immersed in the PDMS reservoir. A bipolar power supply sourced - 1.5 V and +1.5 V at opposite ends of the ITO stripe (outside the PDMS reservoir), creating a linear potential gradient. A thin film of the conducting polymer poly(3,4-ethylenedioxythiophene) doped with p-toluenesulfonate (PEDOT:TOS) was deposited on top of the ITO stripe by vapour phase polymerization (see ESI†). Its conductance was about 100 times lower than that of the underlying ITO stripe, and as a result it replicated the local surface potential of the ITO.

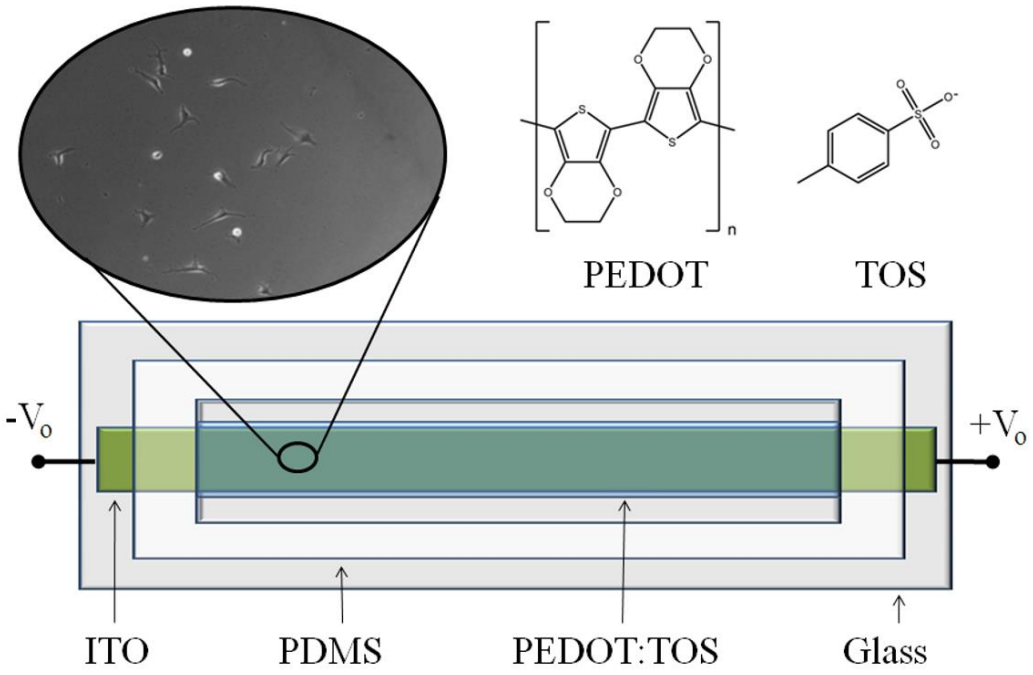

Fig. 2.1: Device schematic and chemical structure of PEDOT:TOS. The inset shows a micrograph of ECs on the PEDOT:TOS surface

The linearity of the gradient was confirmed by measurements of surface potential at several locations along the PEDOT:TOS stripe. The surface potential was found to vary linearly between -1 and +1 V inside the PDMS reservoir. Under this bias configuration, positive ions from the growth medium enter the PEDOT:TOS film near the negatively-biased end. The local hole density decreases in order to maintain charge balance and the film is reduced. In a similar fashion, oxidation takes place near the positively-biased end, creating a redox gradient along the length of the PEDOT:TOS stripe. The redox gradient is accompanied by a characteristic color change across the

film [34]. It should be noted that without the underlying ITO stripe, the change of conductivity associated with ion uptake in the PEDOT:TOS films would result in highly non-linear potential gradients which will fail to cause a well-defined continuum of microenvironments for cell growth.

Cell growth medium was added to the PDMS reservoir and the devices were biased for 1 h to establish the redox gradient on the PEDOT:TOS. The bias was then removed and the cells were seeded. Hence, *cell migration was observed in the absence of applied bias*. The color change that accompanied the establishment of the redox gradient was immediately visible following the application of the bias and remained stable for the duration of the experiment, without noticeable change when the bias was removed. The devices were placed on a Zeiss Axio Observer.Z1m inverted phase contrast microscope stage equipped with a chamber maintained at 37 ˚C, 5% CO_2, and 40% humidity. Cells were plated at a density of 1500 cells mL^{-1} to minimize cell-cell collisions during migration and were allowed to adhere and spread for 6 h prior to observation. Cell migration was measured using time lapse microscopy through a 10x lens, with images taken every 10 min for 6 h. One such image is shown in the inset of Fig. 1. Images were acquired in five locations (‘‘pixels’’) across the PEDOT:TOS stripe that corresponded to an average local potential, as it was applied before seeding the cells, of -0.9 V (reduced), -0.5 V (mildly reduced), 0 V (reference PEDOT:-TOS), 0.5 V (mildly oxidized), and 0.9 V (oxidized). For a control experiment we used a PEDOT:TOS film across which bias was never applied.

Fig. 2.2 shows the trajectories of six cells on the mildly reduced and oxidized pixels. Marked differences in the observed trajectories indicate that the redox state of the polymer significantly affects cell migration. Cells on the mildly reduced pixel seem to only explore their immediate neighborhood, as most of them remain within 100mm from their origin during the 6 h measurement period. On the other hand, cells on the oxidized pixel follow more ‘‘open’’ trajectories, moving as far as 400 mm away from their origin. It should be mentioned that in a control experiment, no spatial differences were observed on EC migration along a device that was not biased.

Cell trajectories were analyzed to extract mean-square displacement $<d^2>$ as a function of time t. Fitting to the persistent random walk equation [35]:

$$< d^2 > = 2S^2P\left[t - P\left(1 - e^{-\left(\frac{t}{P}\right)}\right)\right] \qquad (1)$$

yielded the speed, S, and directional persistence time, P of cells located in each pixel. Fig. 2.3 shows the variation of S and P at the five pixels across the PEDOT:TOS.

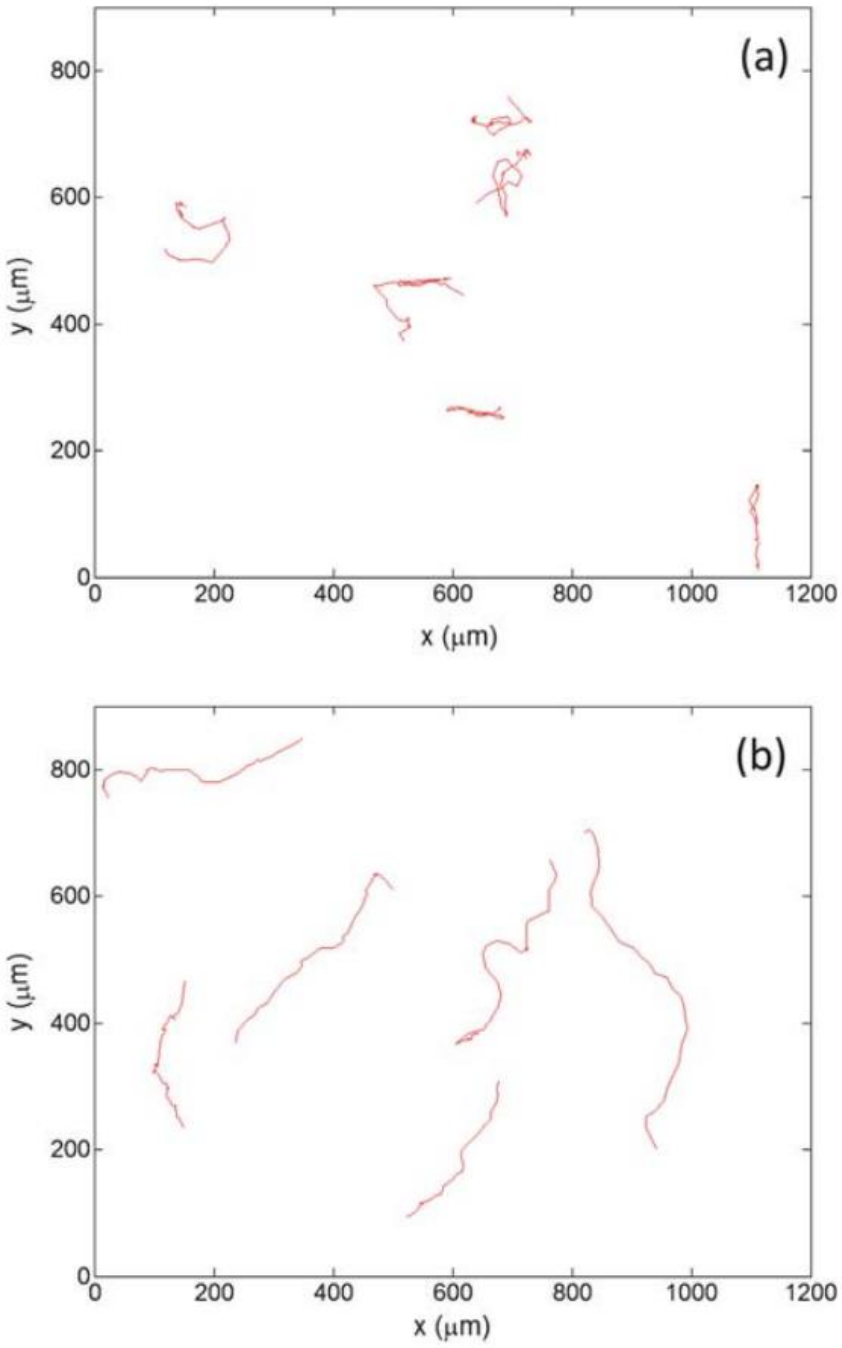

Fig. 2.2: Trajectories of 6 ECs at a mildly reduced (a, V = -0.5 V) and at an oxidized (b, V = +0.9 V) location of the PEDOT:TOS stripe. The potential refers to the average local potential at a PEDOT:TOS pixel, as it was applied before seeding the cells.

The speed for ECs on the reference pixel is 10.8 ± 1.7 μm h^{-1}, consistent with values measured for ECs on glass [36, 37], and on the control PEDOT:TOS film (11.5 ± 1.6 μm h^{-1}). While reduction of PEDOT:TOS does not have a significant effect on speed or persistence, oxidation does: the speed on the oxidized pixel increases to 32.5 ± 3.8 μm h^{-1}, and a similar 3-fold increase is observed in the persistence. These results show that PEDOT:-TOS can be used to electrically control cell migration behaviour. The 3-fold increase in speed achieved by oxidizing the PEDOT:TOS film compares well to improvements measured using fluid shear stress [36, 38] and chemical gradients [37] to induce migration. A larger change might be achievable using a higher applied bias, but electrolysis in the cell medium becomes an issue.

Cell migration involves the formation of new attachments at the front of the cell and the breaking of existing attachments at the rear. As a result, the maximum migration speed is predicted to occur at an intermediate value of cell-substrate adhesiveness [39]. Increasing or decreasing adhesion beyond this optimum is therefore predicted to decrease cell migration speed. Cell adhesion is mediated in part by the adsorption of adhesion proteins (e.g. fibronectin) that are contained in the serum of the growth medium. We therefore conducted an immunostaining assay to quantify the density of adsorbed fibronectin (Fn) at different locations along the PEDOT:TOS stripe. The results, shown in Fig. 4, reveal that the density of adsorbed Fn increases along the PEDOT:TOS stripe from the oxidized to the reduced end. The observed changes in cell speed along the PEDOT:TOS stripe can be understood by assuming

strong EC adhesion on the reduced parts of the PEDOT:TOS stripe. In this limit, cells find it difficult to break existing attachments and their speed is low. The lower density of adsorbed Fn on the oxidized pixels would then decrease cell adhesion, thereby increasing cell speed. This interpretation is consistent with the observation of Paleceket al., who have shown that increasing the density of adsorbed Fn above a certain value decreases cell speed [40].

An alternative interpretation is suggested by two recent studies of cell growth on conducting polymer surfaces [17, 33]. Both studies showed a higher density of attached cells on oxidized than on reduced PEDOT:TOS, suggesting stronger cell adhesion on the oxidized part of the film. However, human serum albumin and Fn were found to adsorb preferentially on reduced PEDOT:-TOS. This was reconciled by hypothesizing that the orientation of the adsorbed protein at the two electrodes is different. According to these reports, the observed changes in speed along the PEDOT:TOS stripe can be understood by assuming that EC adhesion on the reduced parts of PEDOT:TOS stripe is below the optimum. In this limit, cells find it difficult to form new attachments and their speed is low. Stronger cell adhesion on the oxidized PEDOT:TOS pixels increases cell speed. At this point it is not possible to distinguish between these two interpretations and the only conclusion that can be drawn is that the redox gradient on the PEDOT:TOS establishes different microenvironments for cell growth. Understanding the physics of protein adsorption on conducting polymer

surfaces will be a major step towards understanding the changes in migration behaviour observed here.

Adsorbed Fn density gradients, prepared using counter-propagating self-assembled monolayer techniques, are known to direct cell migration through haptotaxis [37, 41]. Not surprisingly, directional cell migration was found to occur along the PEDOT:TOS stripe. Analysis of all cells trajectories on the reference pixel (which is located at the centre of the gradient) shows that there is a net 7.7 mm migration (in 6 h) from the reduced to the oxidized part of the PEDOT:TOS stripe. This displacement is similar in magnitude with values measured on static Fn gradients [37, 41]. However, the direction of cell migration in static gradients is from low to high Fn densities, the opposite to what is observed here. This lends support to the hypothesis of stronger cell adhesion on the oxidized part of the film, as haptotaxis leads cells towards regions of higher adhesion [42].

Compared to other techniques that are used to control cell migration, the device discussed here offers the advantages of simplicity and electrical control, and might yield a useful tool for cell biology. Migration can be slowed down or accelerated, enabling the study of the signal transduction mechanisms governing cell speed, extension, sensing and directionality.

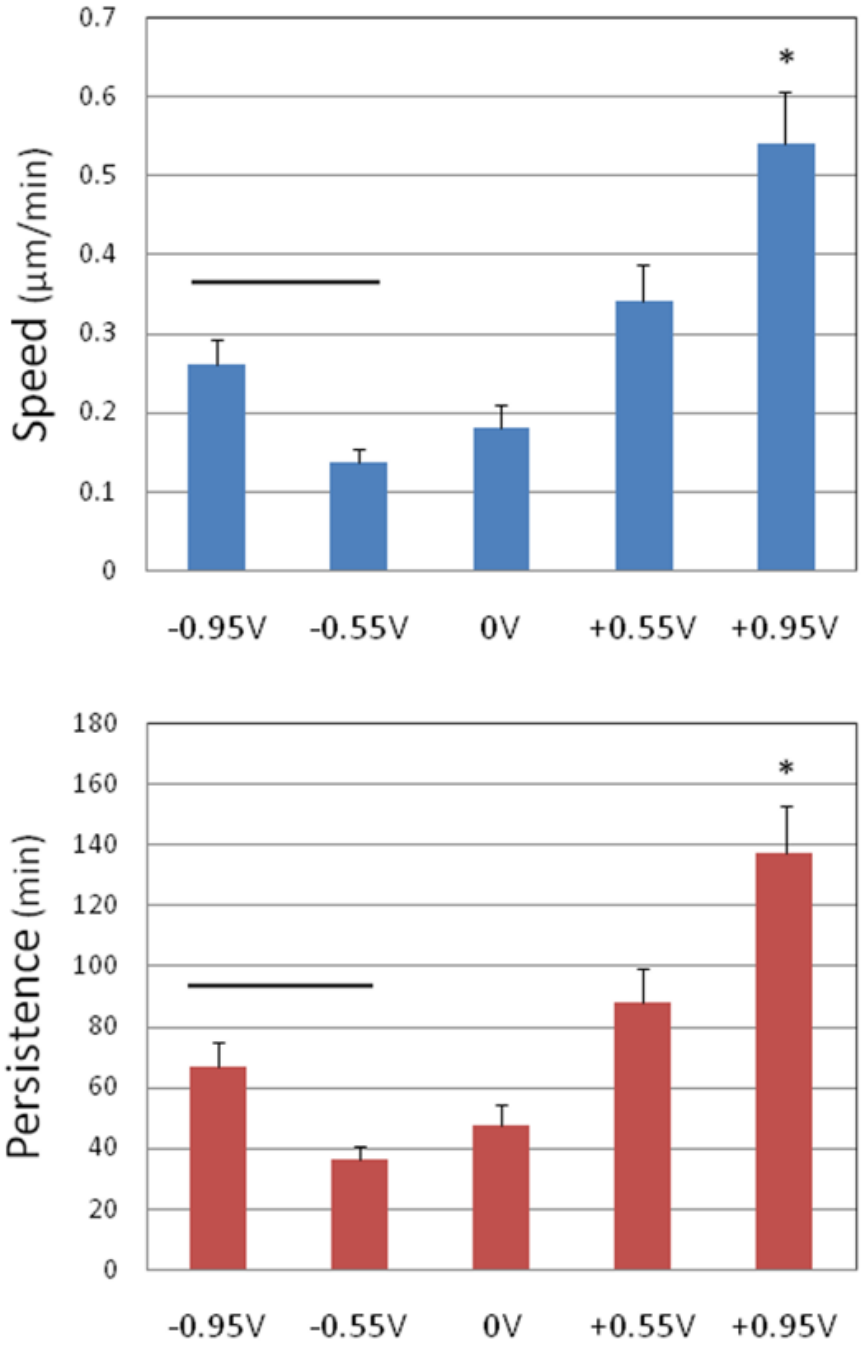

Fig. 2.3: Migration speed and direction persistence time at various locations across the PEDOT:TOS stripe which are marked by the average local potential, as it was applied before seeding the ECs. ‘‘*’’ indicates $p<0.0001$ compared to all other groups. Dash indicates statistically similar groups.

Because these are the same cell behaviours critical to multiple biological processes, including cancer cell metastasis, inflammatory response, wound healing and embryonic development, implementing such a device could lead to the identification and study of molecular targets mediating these processes. Multiple experiments could easily be assembled into one culture dish, enabling the study of multiple treatments and conditions simultaneously. Moreover, the device offers open access to the cells, an advantage over microfluidic techniques. Yet, conducting polymer devices similar to the one reported here have been integrated with both traditional [43] and surface-directed [44] microfluidic channels. Therefore, electrical control of cell migration can also be obtained in a microfluidic format for systems-on-a-chip applications.

Directed migration can be induced without the need for precise patterning of chemical or mechanical cues on a surface –the redox gradient is established automatically and its magnitude, direction, and offset can be controlled by the applied bias. A smaller device, easily achievable with microfabrication, can support a steeper electrical gradient, creating an opportunity to control directional cell migration. PEDOT:TOS is biocompatible [14], and therefore can be incorporated into current biomaterial designs to enhance cell infiltration into tissue engineered constructs. As a wound healing dressing, for example, the use of PEDOT:PSS may decrease healing time by increasing directional cell migration into the wound. Additional opportunities for *in vivo* use in conjunction with other conducting polymer biomedical devices. One example is the blood-vessel connector developed by Micromuscle AB: it consists of a

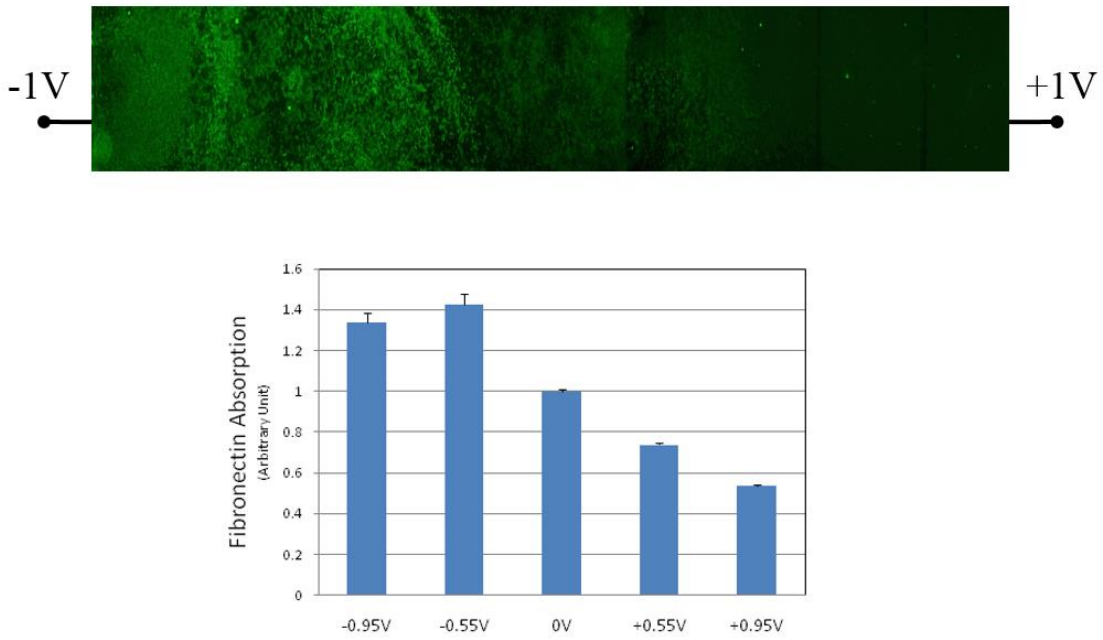

Fig. 2.4: A fluorescent micrograph taken after immunostaining of adsorbed density of fibronectin along the PEDOT:TOS stripe. The direction of applied bias is indicated.

metal/conducting polymer bilayer rolled into a cylinder. When inserted between the ends of severed blood vessels and activated by an applied potential it expands to connect the severed vessel. Our work shows that such devices can be designed to induce directional cell migration, thereby shortening healing time. The examples mentioned above illustrate that the conducting polymer device described here might offer an easy-to-use, tunable platform which could be easily integrated into biomedical devices.

2.5 Conclusions and Perspectives

In conclusion, we discussed a conducting polymer device that achieves a continuum of microenvironments for cell growth to affect the migration behaviour of bovine aortic endothelial cells. Marked differences were observed as a function of location along the polymer stripe, and a 3-fold variation is achieved in cell migration speed and directional persistence time. Directional cell migration along the conducting polymer stripe was induced. A gradient in adsorbed fibronectin indicates that a spatial variation in cell adhesion is at play.

CHAPTER 3

ELECTRICAL CONTROL OF CELL ADHESION USING A CONDUCTING POLYMER DEVICE

3.1 Contributors

This project was a collaboration between the former Malliaras group and Fischbach group in Biomedical Engineering. The study was completed in parallel with the Cell Migration project described in Chapter 2 by utilizing the same device architecture. The majority of the experimental work was carried out by Alwin W. Wan (a former graduate student in the Malliaras group), and Daniel J. Brooks (a former graduate student in Fischbach group.

3.2 Abstract

We describe a conducting polymer device that can induce electrically controlled density gradients of normal and cancerous cell lines, and hence can be used as a tool for the study of cell–cell interactions.

This work was published in *Chemical Communications* in 2009 [15]. All figures reproduced with permission.

3.3 Introduction

Gradients in cell density control the functions of normal and pathological tissues by regulating the quality and quantity of cell–cell interactions. For example, spatial variations in cell density lead to the generation of growth factor gradients, which, in turn, influence cell migration, proliferation, and differentiation [45]. Additionally, gradients in cell density can impact the number of physical connections a cell is able to form with neighboring cells, which modulate intracellular signaling pathways and affect cell behaviour [46]. Perturbation of cell interactions in normal tissues (e.g., due to injury) typically triggers a cascade of events that re-establishes tissue homeostasis. However, in pathological tissues (e.g., tumours) these control mechanisms are dysfunctional and can lead to impaired tissue functions and patient prognosis [47]. The ability to establish controllable cell density gradients is critical to gaining a better understanding of the underlying cellular and molecular mechanisms.

A variety of techniques can be used to generate spatially controlled variations in cell density. For example, artificial, growth factor-sequestering extracellular matrices allow to probe the synergy between interstitial fluid flow and growth factor signalling on the formation of endothelial cell gradients [48]. Additionally, microfluidic devices capable of generating morphogen gradients provide useful tools to establish local variations in cell density as a result of directed cell migration [49]. These systems permit to establish gradients in cell density as a function of varying

mechanical and chemical cues, but whether electrical stimuli may be used in a similar manner has not been investigated.

In 1994, Wong *et al.*, discovered that aortic endothelial cells grow differently on oxidized and on reduced polypyrrole films [32]. Since conducting polymers such as polypyrrole can be reversibly switched between oxidized and reduced states, these experiments pave the way for non-invasive control of cell growth. Subsequent work focused predominantly on neurons, where the stimulation of neurite outgrowth is important for, among other things, repair of spinal cord injury [50]. The topic of cell growth on conducting polymer surfaces is currently receiving renewed attention due to the interest in organic electronics [27]. A recent example is the work by the Berggren group demonstrating differences in neural cell adhesion on reduced and on oxidized conducting polymer electrodes [33].

3.4 Results and Discussion

In this communication we report a device in which an applied bias causes a redox gradient in a conducting polymer film, which, in turn, leads to the creation of density gradients in normal and cancerous cells. We chose two cell lines that are representative models of normal and cancerous cells for this demonstration: the 3T3-L1 (ATCC CL-173) cell line, which consists of mouse fibroblasts capable of transforming into adipocytes and is representative of normal mesenchymal cells, and the MDA-MB-231

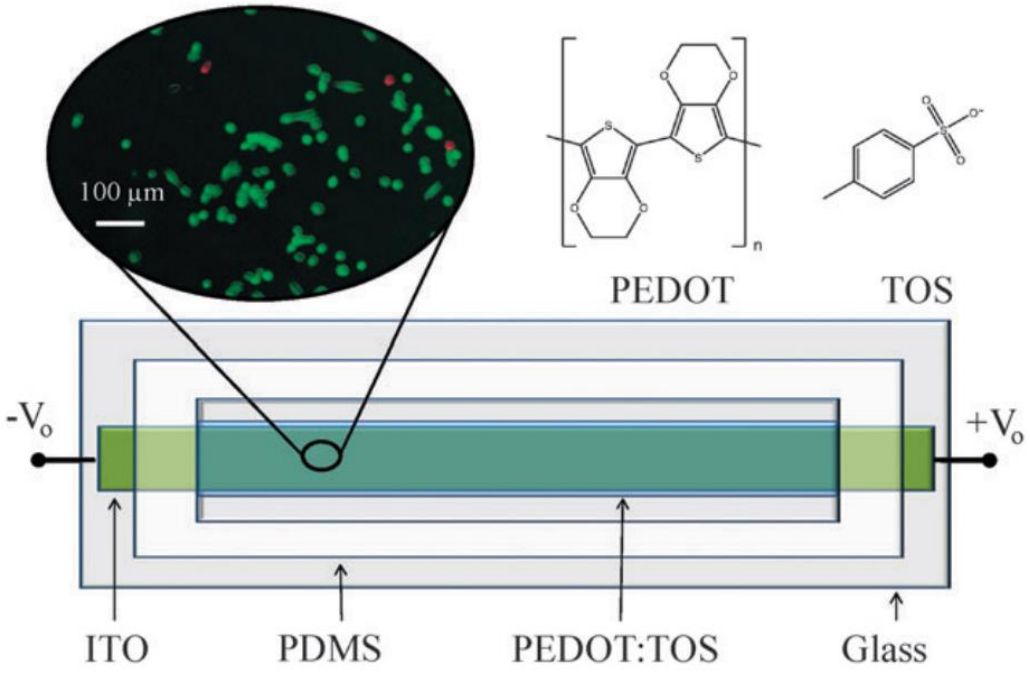

Fig. 3.1: Device schematic and chemical structure of PEDOT-TOS. The inset shows a micrograph of MDA-MB-231 cells after performing a live/dead assay.

(ATCC HTB-26) cell line, which is derived from human breast cancer and is representative of an aggressive and invasive form of the disease.

Fig. 1 shows the device that was used to create the redox gradients. A 3 mm wide, 2.5 cm long indium tin oxide (ITO) stripe was deposited on a glass substrate, onto which a PDMS reservoir that contained the cell growth medium was attached. A ground electrode was immersed in the PDMS reservoir. A bipolar power supply sourced - 1.5 V and + 1.5 V at opposite ends of the ITO stripe (outside the PDMS reservoir), creating a linear potential gradient. A thin film of the conducting polymer

poly(3,4-ethylenedioxythiophene) doped with p-toluenesulfonate (PEDOT–TOS) was deposited on top of the ITO stripe by vapour phase polymerization [51]. Its conductance was about 100 times lower than that of the underlying ITO stripe, and as a result it just replicated the local surface potential of the ITO. The linearity of the gradient was confirmed by measurements of surface potential, which was found to vary inside the PDMS reservoir between - 1 and + 1 V. Under this bias configuration, positive ions from the growth medium enter the PEDOT–TOS film near the negatively-biased end. The local hole density decreases in order to maintain charge balance and the film is reduced. In a similar fashion, oxidation takes place near the positively biased end, creating a redox gradient along the length of the PEDOT–TOS stripe. The redox gradient is accompanied by a characteristic colour change across the film [34]. It should be noted that without the underlying ITO stripe, the change of conductivity associated with ion uptake in the PEDOT–TOS films would result in highly non-linear potential gradients which might lead to ill-defined redox gradients.

Cell growth medium was added to the PDMS reservoir and the devices were biased for 1 hour to establish the redox gradient on the PEDOT–TOS. The bias was then removed and the cells were seeded. Hence, cell growth took place in the absence of applied bias. The colour change that accompanied the establishment of the redox gradient was immediately visible following the application of the bias and remained stable for the duration of the experiment, without noticeable change when the bias was removed. Cells were seeded on the device and allowed to grow for 24 hours before

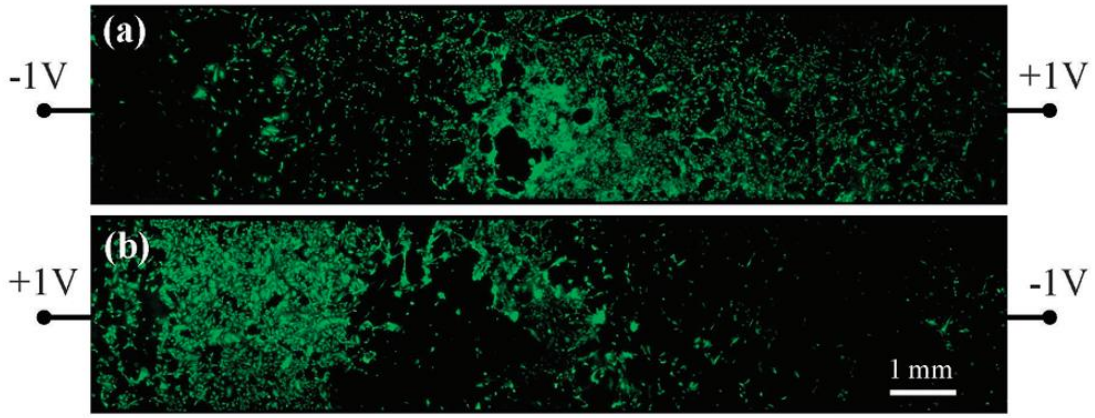

Fig. 3.2: Fluorescence micrographs of calcein-green stained 3T3-L1 cells for two devices biased in opposite directions.

their viability was quantified with a live/dead assay, using calcein AM (green, calcein acetoxymethyl ester; Invitrogen C1430) for live cells, and propidium iodide (red, Sigma-Aldrich P4170) for dead cells. Seeding densities were ~15 000 cells per cm^2 for the 3T3-L1 cells and ~30 000 cells per cm^2 for the MDA-MB-231 cells.

Fig. 3.2 shows composite images mapping 3T3-L1 cell distributions along the PEDOT–TOS stripe in two devices that were biased in opposite directions from each other. Each composite consists of 6 individual fluorescence micrographs, obtained through a 2.5x objective with a Zeiss Axio Observer.Z1 microscope. The images reveal regions of low cell density, where individual cells are well separated from each other, as well as regions where the cells are beginning to form a confluent monolayer. From these plots it can be seen that large density gradients can indeed be established on the PEDOT–TOS surface. Moreover, in both plots, the regions of low density are close to

the negatively-biased side of the PEDOT–TOS. Therefore, the direction of the cell density gradient is controlled by the direction of the applied bias.

Fig. 3.3 shows population densities obtained from analysis of fluorescence images from both 3T3-L1 and MDA-MB-231 cells. The images were parsed in 20 segments along the length of the PEDOT–TOS stripe and the number of individual cells was counted using ImageJ (National Institutes of Health). The average cell density, obtained from analysis of data from two devices, was then plotted as a function of the average local potential that was applied on each segment before seeding the cells. The experiment was repeated several times to ensure the reproducibility of these observations. The data show that both types of cells prefer the oxidized side of the PEDOT–TOS film, and the cell density decreases gradually towards the reduced side of the film. It should be noted that quantification of the total cell surface area at different locations of the established cell density gradient yielded similar results.

The observed density gradients are not caused by a change in the viability of the cells along the PEDOT–TOS film. The inset of Fig. 1 shows a typical micrograph (phase-contrast, green and red fluorescence at 10x) of the MDA-MB-231 cells from a reduced region of PEDOT–TOS after performing the live/dead assay. In this image green fluorescence corresponds to live and the red to dead cells, indicating that the majority of the cells are alive. Cell viability was found to exceed 98 ± 1% regardless

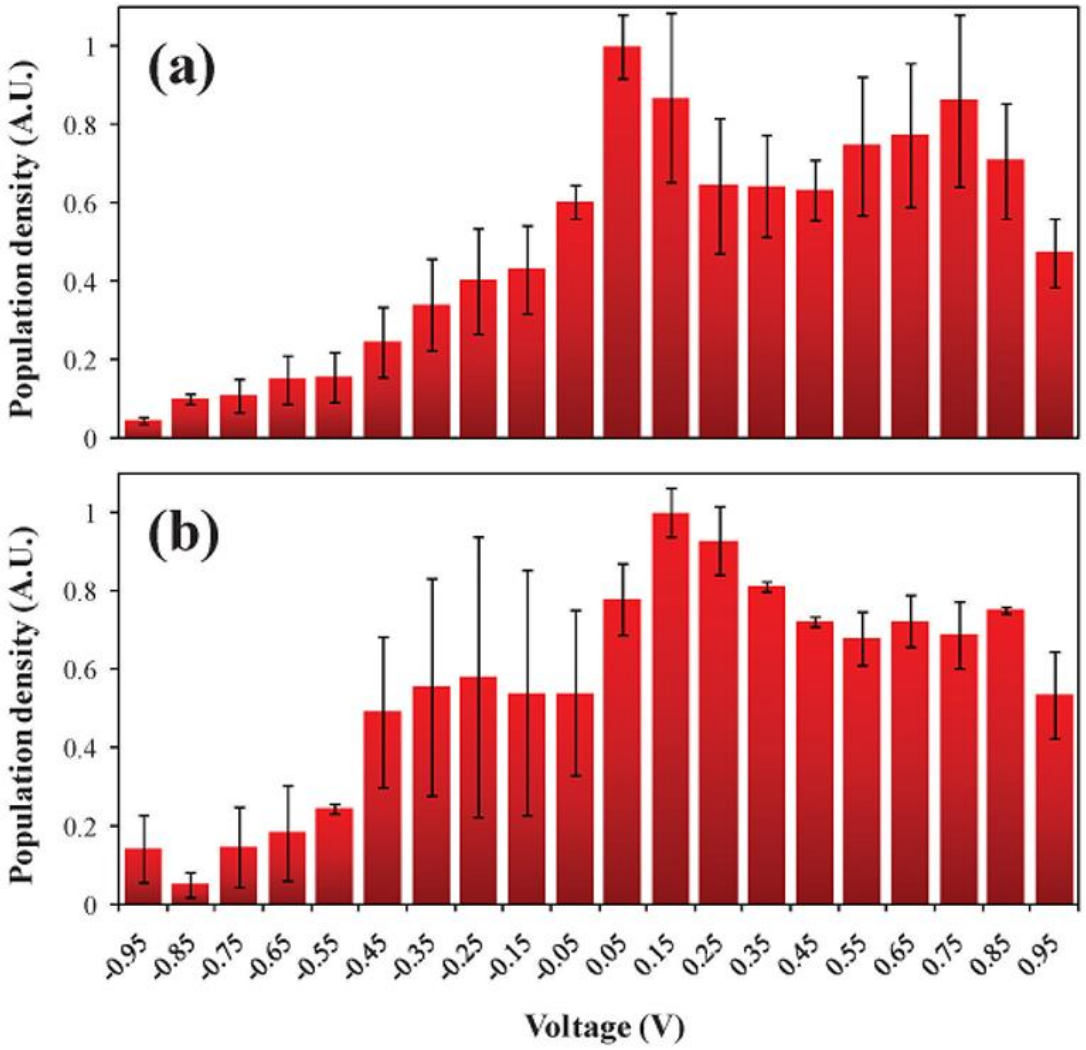

Fig. 3.3: Population densities for the 3T3-L1 cells (a) and the MDA-MB-231 cells (b) across the PEDOT–TOS film.

of the redox state of the PEDOT–TOS film. The 3T3-L1 cells also showed similarly high viability on all regions of the PEDOT–TOS film. Cells grown on a control device that was never biased also showed the same viability. It should be noted though that if the applied bias is not removed prior to seeding the cells, their viability and morphology

are quickly and adversely affected. In an experiment where the bias was maintained during cell culture, changes in cell morphology were detectable less than 30 minutes after seeding. After less than 2.5 hours of culture, nearly all adhered cells on the device had lost viability, as confirmed with a live/dead assay.

It is likely that the observed cell density gradients arise due to differences in cell adhesion. The latter is mediated in part by the adsorption of adhesion proteins (*e.g.* fibronectin) that are contained in the serum of the growth medium. An immunostaining assay was performed to quantify fibronectin (FN) adsorption on different locations of the device. Devices were incubated under bias for 1 hour in a FN solution diluted in DI water. The concentration of FN corresponded to an area density of 15 μg cm^{-2} for each device. The FN was fixed with neutral-buffered formalin for 30 minutes and the devices were washed twice in phosphate buffered saline (PBS) with 0.5% bovine serum albumin (BSA) to prevent non-specific binding of the primary antibody. The devices were then incubated for 1 hour in a 1 : 400 dilution of the anti-fibronectin primary antibody in PBS–BSA. The devices were washed twice with PBS–BSA and incubated for 1 hour in the dark in a 1 : 100 dilution of a fluorescent goat anti-rabbit secondary antibody in PBS–BSA. Subsequent washing and imaging of the fluorescence from the secondary antibody revealed the relative concentration of adsorbed fibronectin. The data were corrected for the dependence of the optical density of PEDOT–TOS on its redox state and are shown in Fig. 4. The control corresponds to a device that was never biased. The data show that a redox gradient across a PEDOT–TOS film causes a

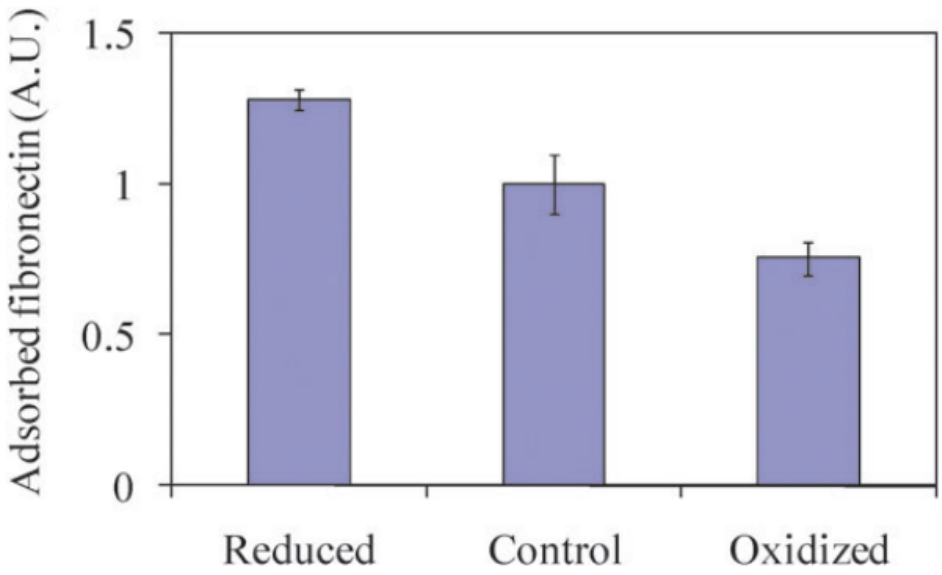

Fig. 3.4: Quantification of adsorbed fibronectin as a function of the redox state of PEDOT–TOS.

gradient in adsorbed fibronectin concentration, with concentration decreasing from the reduced towards the oxidized side.

The higher concentration of adsorbed fibronectin on the reduced side of the device would imply better cell adhesion, leading to a higher cell density [52], which is the opposite of what we find here. The reason for the higher cell density on the oxidized side of PEDOT–TOS is currently not understood. A similar finding was recently reported by the Berggren group [33]. In a study of adhesion of c17.2 neural stem cells on reduced and oxidized conducting polymer electrodes, they showed a higher density of attached cells on the oxidized electrode. Moreover, they also showed that human serum albumin adsorbs preferentially to the reduced electrode. It was hypothesized that

the orientation of adsorbed protein at the two electrodes might be different, or that the higher protein concentration on the reduced electrode might have a blocking effect on extracellular matrix proteins and hinder cell adhesion [33]. Understanding the physics of protein adsorption on conducting polymer surfaces will be a major step towards uncovering the pathways leading to non-invasive, electrical control of cell adhesion.

The device described here can create cell density gradients that range from isolated, well-spaced cells to confluent monolayers, and these are suitable for the study of cell–cell interactions. Compared to other techniques that can yield similar cell density gradients, it offers the advantages of simplicity and electrical control. There is no need for precise patterning of chemical cues on a surface—the redox gradient is established automatically and its direction can be controlled by the applied bias. The spatial extent of the gradient (here, ~ 1 cm long) can be controlled by the dimensions of the conducting polymer film, or the applied bias. Moreover, the device described here offers open access to the cells—an advantage over microfluidic techniques. Yet, conducting polymer devices similar to the one reported here have been integrated with microfluidic channels [44]. Therefore, electrical control of cell density gradients can also be obtained in a microfluidic format for systems-on-a-chip applications.

3.5 Conclusions and Perspectives

We described a simple device that can be used to establish redox gradients on a conducting polymer film. When cells are cultured on this film, density gradients are established. This was demonstrated for both normal and cancerous cells. A variation in the density of adsorbed fibronectin implies that the device works by controlling cell adhesion.

CHAPTER 4

REAL-TIME *IN VIVO* URIC ACID BIOSENSOR SYSTEM FOR BIOPHYSICAL MONITORING OF BIRDS

4.1 Abstract

Research on birds has long played an important role in ecological investigations, as birds are relatively easily observed, and their high metabolic rates and diurnal habits make them quite evidently responsive to changes in their environments. A mechanistic understanding of such avian responses requires a better understanding of how variation in physiological state conditions avian behavior and integrates the effects of recent environmental changes. There is a great need for sensor systems that will allow free-flying birds to interact with their environment and make unconstrained decisions about their spatial location at the same time that their physiological state is being monitored in real time. We have developed a miniature needle-based enzymatic sensor system suitable for continuous real-time amperometric monitoring of uric acid levels in unconstrained live birds. The sensor system was constructed with Pt/Ir wire and Ag/AgCl paste. Uricase enzyme was immobilized on a 0.7 mm sensing cavity of nafion/cellulose inner membrane to minimize the influences of background

This work was published in *Analyst* 2014 [101]. All figures reproduced with permission.

interferents. The sensor response was linear from 0.05 to 0.6 mM uric acid, which spans the normal physiological range for most avian species. We developed a two-electrode potentiostat system that drives the biosensor, reads the output current, and wirelessly transmits the data. In addition to extensive characterization of the sensor and system, we also demonstrate autonomous operation of the system by collecting *in-vivo* extracellular uric acid measurements on a domestic chicken. The results confirm our needle-type sensor system's potential for real-time monitoring of birds' physiological state. Successful application of the sensor in migratory birds could open up a new era of studying both the physiological preparation for migration and the consequences of sustained avian flight.

4.2 Introduction

Research on birds plays a large role in investigations related to ecology, evolution and behavior. Birds are diurnal and visual, and they are readily observable and trackable for a great variety of research in the field. Their high metabolic rates make them highly responsive to their environments, and they therefore tend to be good indicators of environmental change [12]. The current state-of-the-art for avian physiological monitoring in the field is to take blood samples upon capture, yielding a "snap shot" of information on the covariation of metabolites and hormones with the phases of migration and breeding in wild birds [53-57]. The metabolism of individual birds over the course of their annual migrations or for their once in-a-lifetime dispersal event is still poorly understood because of the difficulties of studying birds that travel tens to

thousands of kilometers in their movements [54]. The ability to track and study migratory birds has increased in recent years with the development of new generations of radio-tags and data-loggers capable of increasingly precise monitoring of bird's dynamic locations [8, 58, 59]. A system that can combine this positional tracking data with a real-time dynamic measurement of the physiological state of the birds could open up an entirely new way of studying avian movement biology and behavior. For example, being able to track physiological changes and location in a single moving bird could yield priceless information on its internal state and location-associated environmental conditions to enable an unprecedented understanding of the movement-decision-making of individual birds.

Metabolite sensing and quantification in capillary blood is a well-established technology. The vast majority of existing technologies are based around an enzymatic reduction of the target metabolite and detection of the products such as glucose [60-62], cholesterol [63], or lactic acid [64-66]. In general, the importance of these measurements to human health monitoring (in particular glucose monitoring for type 1 diabetes) has led to the development of a large diversity of robust, commercially available devices [67]. Despite the wealth of data on blood chemistry, placing sensors in blood vessels presents difficult challenges for sensor placement and attachment as well as for the life-time of the sensor, which tends to get fouled by defensive cells in the blood. A major recent advancement that has enabled the deployment of real-time continuous versions of these systems has the ability to accurately determine glucose

levels from measurements made in the interstitial space between capillaries, rather than sampling the blood directly [68, 69]. This has led to the development of implantable biochips, which enable continuous monitoring of glucose and lactate levels to influence patient outcomes following trauma-induced hemorrhage [64]. Implantable electrochemical sensors have also been used for *in-vivo* biosensing applications in animals such as glucose monitoring in fish [61] and continuous alcohol monitoring in a Wistar rat [70].

Because birds' energy pathways are dominated by lipid rather than carbohydrate metabolism, variation in somatic glucose levels are not as informative as they are in mammalian systems. Glucose levels do not change, for example, over the full range of physiological states shown by arriving and refueling godwits on a migratory stop-over in the Wadden Sea [71]. By contrast, uric acid is a good indicator of protein catabolism in birds since its presence in the body is a consequence of the breakdown of protein, either from recently ingested proteinaceous food or from catabolism of body protein [72]. There are various approaches to be able to detect uric acid levels: chemiluminescence [73], spectrophotometry [74], fluorescence [75] and electrochemistry [76]. In general, electrochemical methods for detecting uric acid can be classified as either non-enzymatic or enzymatic methods. Enzyme-based electrochemical methods are preferred due to their high selectivity and sensitivity [77, 78]. In most of these methods, determination of uric acid is performed by oxidation of enzymatically generated H_2O_2 at the sensing electrode [79]. Uricase enzymes are

immobilized onto various modified electrodes such as polyelectrode multilayer films [80], Iridium-modified carbon electrode [81], polypyrrole and polyaniline film [82, 83], eggshell membrane [84], polyaniline-multiwalled carbon nanotube composite film [85], zinc oxide nanowires [77] and o nano-particle/multiwalled carbon nanotube layer deposited on gold electrode [86]. Although these methods have focused on parameters such as simplicity, sensitivity, low detection limit and low cost, none of them has been able to implement uric acid sensing for *in-vivo* applications.

Here for the first time, we have developed a miniature needle-type enzyme sensor system suitable for real-time amperometric monitoring of uric acid in birds. The biosensor uses uricase enzyme to catalyze the uric acid reaction, and reduces the produced hydrogen peroxide at the sensing cavity, where it is detected amperometrically with good sensitivity and stability characteristics. We have also designed and integrated our sensor with a two-electrode wireless potentiostat system. Finally, we demonstrate the *in-vivo* monitoring of uric acid in a domestic chicken.

4.3 Experimental

4.3.1 Structure of uric acid sensor

The uric acid sensor, shown in Fig. 4.1, was designed similar to previous needle type *in-vivo* glucose sensors [60-62]. The sensor was made using Teflon coated platinum-iridium (Pt/Ir; 10%) wire (0.125 mm o.d.; Advent Research Materials Ltd, Oxford,

England). It was stripped at one end to create a sensing cavity of 1 mm. The tip of the wire was sealed with epoxy resin. Silver wire (0.1 mm o.d., from Sigma Aldrich, St. Louis, MO) was wrapped around the Teflon coated surface. Ag/AgCl paste (CH Instruments Inc, USA) was applied onto the sensor body to create a reference/counter electrode. Following that, the sensing cavity was degreased with acetone, isopropyl alcohol, and deionized water to strip any coating residues before inner membrane deposition.

To prevent changes in other species (e.g., ascorbic acid and glucose) from influencing the sensor output, the Pt/Ir electrode was coated with an inner membrane composed of Nafion and CA. Twelve alternating coatings of Nafion and CA were found to be sufficient to eliminate the interfering species effectively. Uricase enzyme was immobilized on the coated electrode and crosslinked with glutaraldehyde to protect the enzyme layer from heat degradation, proteolytic enzymes and hydrolysis [87]. The sensing cavity was first coated with two thin layers of Nafion by dipping it into a well containing 5% Nafion and air-drying for 10 min between each coating. After Nafion coating, the sensor was coated with two thin layers of CA by dipping it into the 5% CA solution in 2:1 acetone-ethanol for 5 s followed by drying at room temperature for 10 min between coat. This Nafion and CA deposition cycle was repeated 2 additional times. Uricase enzyme was immobilized on the working electrode by absorption on inner membranes. 0.7 µL of freshly prepared enzyme solution containing 1% uricase,

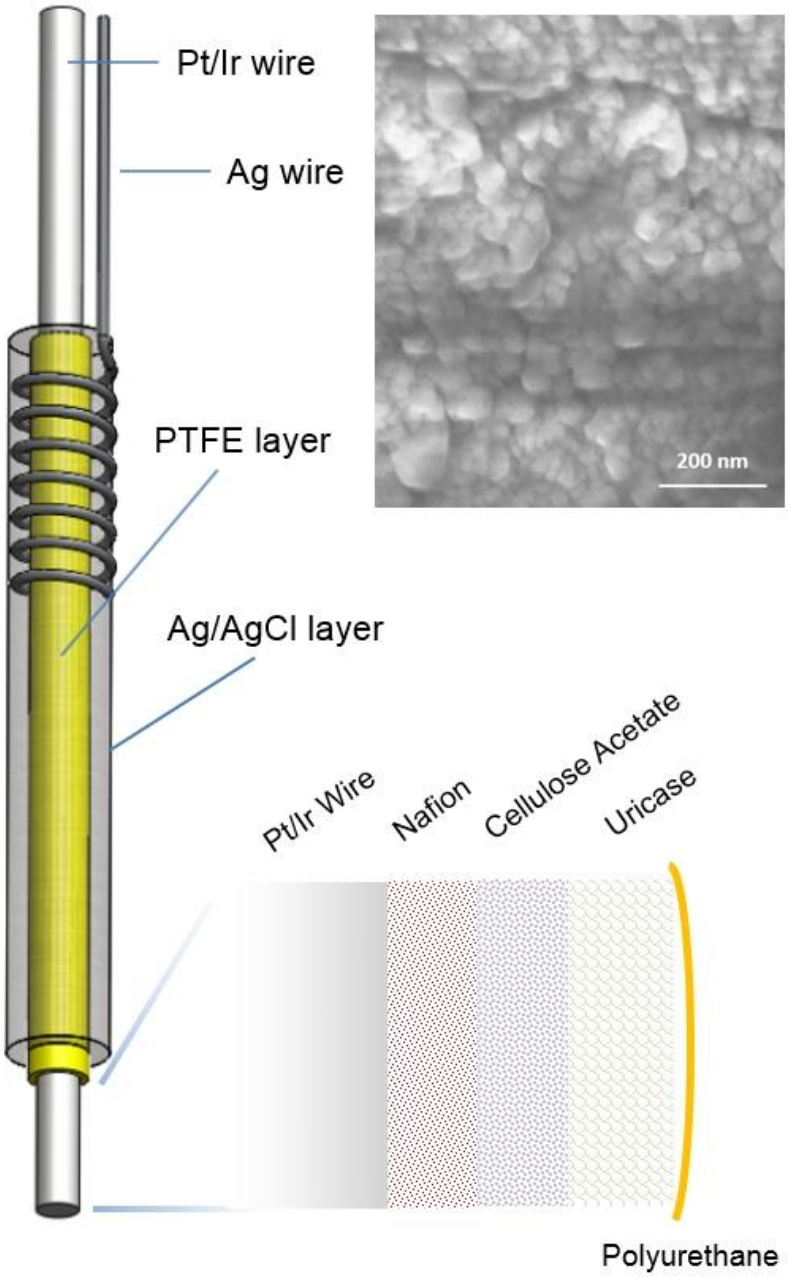

Fig. 4.1: View of needle type in-vivo enzymatic uric acid biosensor, inset shows the SEM image of the sensing cavity of the biosensor containing immobilized uricase enzymes.

0.6% bovine serum albumin and 0.4% glutaraldehyde was transferred to the sensing cavity while the sensor was held in a horizontal position.

Uricase enzyme was immobilized on the working electrode by absorption on inner membranes. 0.7 µL of freshly prepared enzyme solution containing 1% uricase, 0.6% bovine serum albumin and 0.4% glutaraldehyde was transferred to the sensing cavity while the sensor was held in a horizontal position. The sensor was then allowed to dry for 1 hr. A polyurethane (PU) outer layer was deposited around the entire sensor to prevent degradation of the sensor and to make the output current independent of external mass transfer by serving as a rate-limiting barrier for diffusion [65]. Using the wire loop technique, 5% polyurethane (PU) solution was prepared in 98% tetrahydrofuran (THF)-2% dimethylformamide (DMF). Three turns of wire loop (3 mm inner membrane) were constructed from copper wire (0.5 mm outer diameter) and the inside of the loop was filled with 17 µL PU solution. The whole sensor passed through this loop horizontally which enabled uniform deposition of the outer layer. The sensor was then cured in air for 12 hours and then stored in 0.01 M phosphate buffered saline (pH 7.4) for 7 days to permit outer layer conditioning

4.3.2 In-vitro sensor characterization

In-vitro evaluation of the sensor characteristics was carried out in a 1.5 mL cell at room temperature (25˚C). All in-vitro measurements were conducted in 0.1M PBS (pH 7.4) and dissolved oxygen was saturated with stirring. A potential of +650 mV was applied

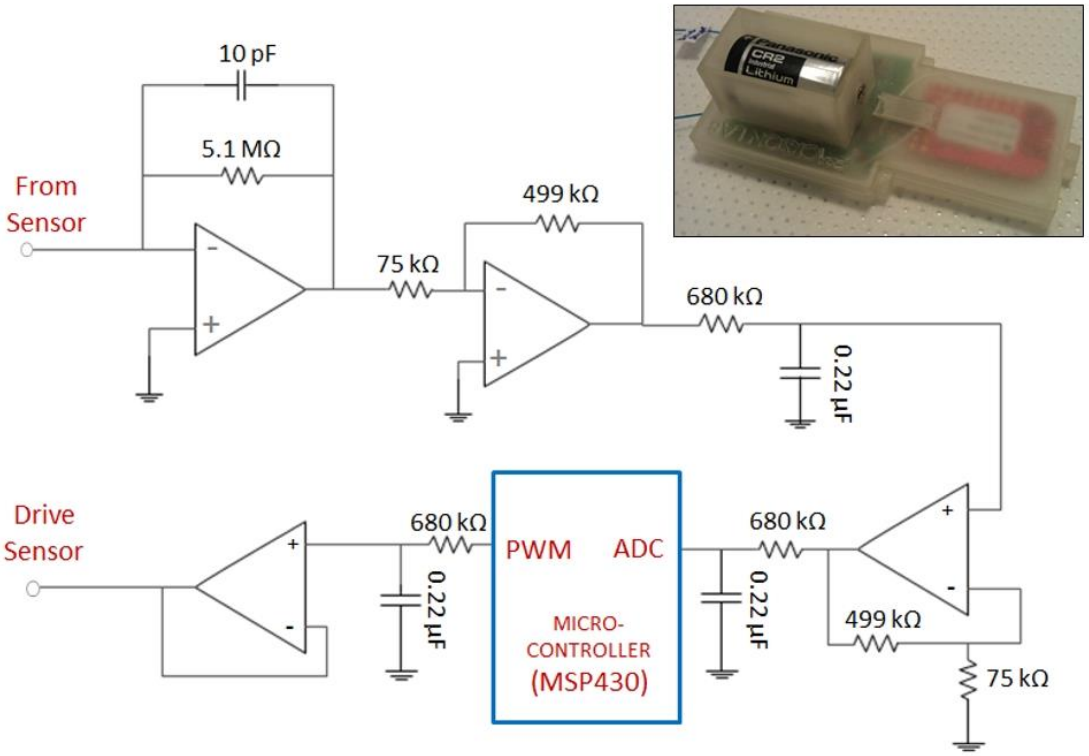

Fig. 4.2: Two electrode potentiostat system used to drive the uric acid biosensor at 650 mV and read the output current (1-20 nA) in real time.

between the working and the reference/counter electrodes by using a Keithley 2400 SourceMeter (Keithley Instruments Inc., OH, USA) for amperometric detection. The background output current was stabilized for 30 minutes before first measurement. The resulting current data were collected by a digital acquisition card installed in a PC controlled with LabView software (National Instruments Corp., Austin, TX). To carry out the calibration of the sensor, increasing amounts of uric acid (or interferent) solutions were injected into the cell with a pipettor every 3 minutes, which was enough

time to get steady-state response. The sensors were stored in 0.01 M phosphate buffer, pH7.4, at 4˚C when not in use.

4.3.3 Two-electrode potentiostat system for in-vivo measurements

By combining a low power microcontroller (MCU) MSP430F2274 (Texas Instruments, TX), amplifiers (Maxim Integrated, CA), and filter blocks, we formed a two-electrode potentiostat system that drives the biosensor at 650 mV [88]. It reads the ultra-low output current of the sensor (1 to 20 nA) and transmits the corresponding voltage data to the base microcontroller connected to a remote computer (Fig. 4.2). We chose low power, low noise MAX407 op-amps (Maxim Integrated, CA) to build amplifiers and filter blocks. Since MAX407 op-amp has a very high input impedance and low input bias current, it was suitable for a two-electrode potentiostat system application. We build the circuit with a minimum number of components to keep the circuit board area small. A Pulse amplitude modulated (PWM) signal from the MCU was converted to DC voltage by low-pass filtering for driving the sensor after buffering. Since the sensor output current is very small, we amplified and converted it to voltage using a transimpedance amplifier, so that it could be measured by the microcontroller's analog to digital converter (ADC). Data was transferred to a base station using an integrated CC2500 2.4 GHz wireless transceiver and recorded to a computer for further analysis.

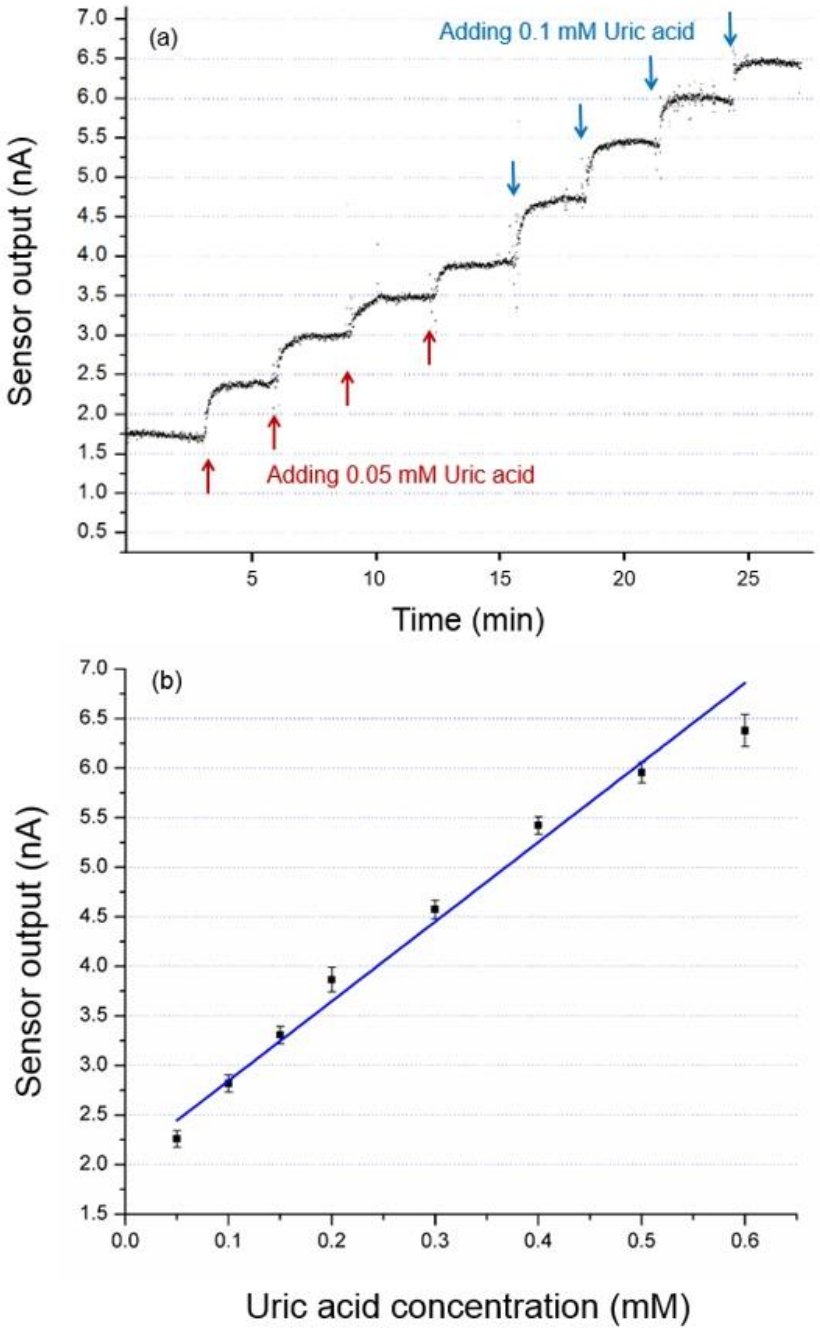

Fig. 4.3: a) In-vitro calibration of the uric acid biosensor by adding various concentrations of uric acid over the expected physiological range. b) Linear fit of the in-vitro uric acid calibration data. Error bars are the standard deviation of the sensor output after stabilization

4.3.4 In-vivo experiments for monitoring interstitial uric acid levels in a domestic chicken

To evaluate the *in-vivo* performance of the sensor, experiments were done on an adult chicken. Feathers in the dorsal feather tract, anterior of the uropygial gland, were clipped at their bases and the skin disinfected using Betadine Antiseptic Solution (Purdue Pharma L.P., NJ). A 20-gauge catheter consisting of an outer polyurethane layer and inner puncture needle (Terumo Medical Corporation, NJ) was inserted slightly over 1 cm immediately beneath the skin without anesthesia. After removing the inner puncture needle, the excess catheter was cut just above the skin. The uric acid sensor was then inserted into the flexible polyurethane outer layer and secured with sterile Tegaderm® film (3M Corporate, MN). Then the wireless two-electrode potentiostat tag was attached directly over the inserted sensor and fastened to the back with a Rappole harness [89] made of dental floss and tightened around the bird's femurs through holes at the sides of the tag case.

Prior to the experiment, the chicken was fasted for 6 hours, lowering the baseline uric acid levels. A blood sample was taken from the chicken before installing the biosensor tag. After installing the tag, we waited 10 minutes for sensor current to stabilize. Then the bird was allowed to eat in order to increase its uric acid levels. Then the bird was allowed to eat in order to increase its uric acid levels. The system collected data for a total of one hour. Before removing the sensor tag, a second blood sample was taken.

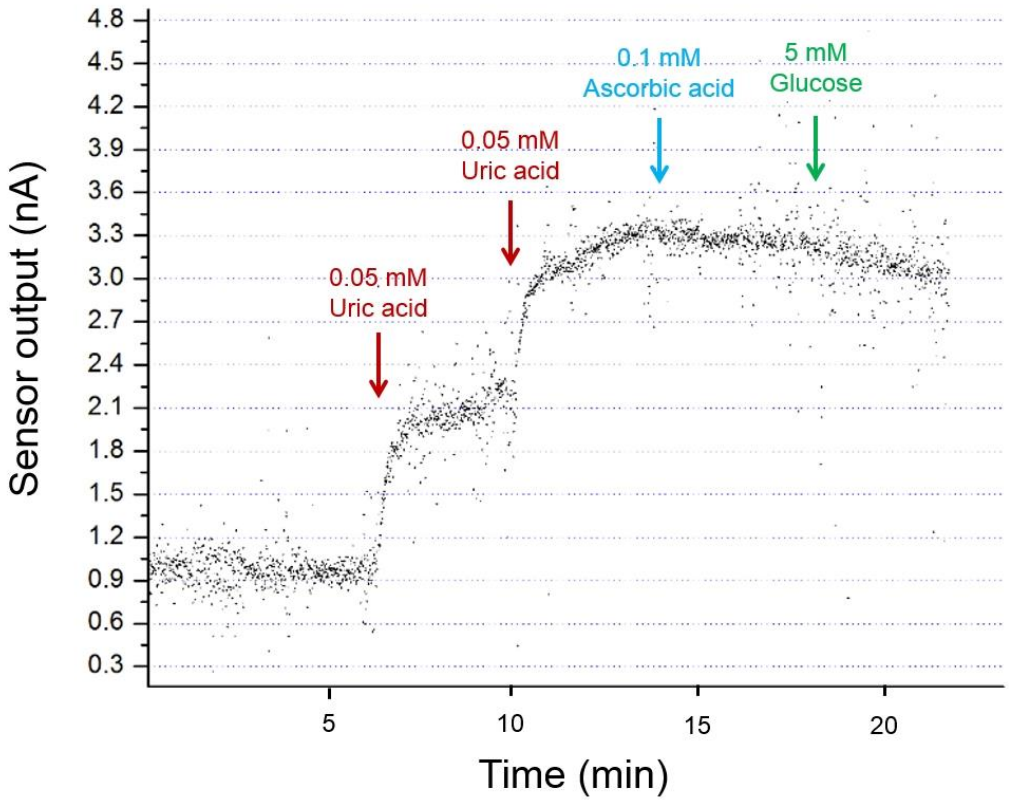

Fig. 4.4: Interference effect on the response of uric acid biosensor, addition of 0.1 mM ascorbic acid and 5 mM glucose did not result in detectable changes in the sensor response

We determined the uric acid levels of two blood samples taken before and after feeding the bird by using a uric acid kit reagent set (Teco Diagnostics, CA) and spectrophotometer (Molecular Devices LLC, CA). We compared the biosensor output to the uric acid level data from the uric acid kit. We then used a two-point calibration method for uric acid level estimation 18. For the change in uric acid levels (U) from U_1 to U_2 (in mM), and the corresponding sensor output currents (I_1 and I_2 in nA), sensor

sensitivity S will be $(I_2 - I_1)/(U_2-U_1)$ and the theoretical sensor output I_0 (which would be observed in absence of uric acid) will be $I_1-(S(G_1))$.

4.4 Results and discussion

4.4.1 In-vitro sensor characterizations

The needle-type UA biosensor is shown in Fig. 1. Uricase catalyzes the oxidation of uric acid to allantoin in the presence of oxygen, producing CO_2 and H_2O_2 simultaneously. A 650 mV potential is applied to the Pt/Ir working electrode with respect to the Ag/AgCl reference electrode. Hydrogen peroxide is reduced on the working electrode surface when potential is applied. This generates a current which is then measured amperometrically. Characterization of the sensor uses 0.1 M phosphate buffer solutions doped with various concentrations of uric acid in the range of expected physiological state.

$$Uric\ acid + O_2 \xrightarrow{Uricase} allantoin + CO_2 + H_2O_2 \quad (1)$$

$$H_2O_2 \rightarrow O_2 + 2H^+ + 2e^- \quad (2)$$

The sensor has a fast response time, and output current reaches steady state levels in less than 60 seconds. This is an important property for real-time *in-vivo* measurements. The sensor has good sensitivity for UA and the sensor output is linear from 0.05 mM

to 0.6 mM UA (Fig. 3). UA levels in avian blood vary from around 0.1 mM to 0.65 mM [90], and our biosensor thus has the ability to detect the complete range of normal uric acid levels in birds. The polyurethane membrane served as a rate-limiting barrier for diffusion of uric acid to the enzyme layer and helped to get a linear dynamic output current range independent of external mass transfer [65].

Electrochemical interference is one of the major problems in biological determination of uric acid since it has a similar oxidation potential to hydrogen peroxide. To prevent the effects of potentially interfering species, the Pt/Ir electrode was coated with inner membranes of alternating Nafion and cellulose acetate (CA). These polymers are negatively charged and inhibit the diffusion of anionic species [60, 91]. In order to test the selectivity achieved, the performance of the UA sensor was tested against interference from ascorbic acid and glucose. As shown in Fig. 4.4, addition of 0.1 mM ascorbic acid and 5 mM glucose did not result in detectable changes in sensor response. We have also tested our biosensor against 0.05 mM L-cysteine and 0.2 mM fructose, which also didn't cause any changes in the sensor response. We observed slight decreases in current output from the dilution of the uric acid solution with ascorbic acid and glucose standard solutions, but the sensor still was able to detect UA reliably. Clearly, the uricase enzyme retains its activity and a good turn-over time after immobilization, so it has the ability to deliver fast response to small changes in UA concentrations. This results show that our biosensor system gives a sensitive response to uric acid by rejecting the interferences.

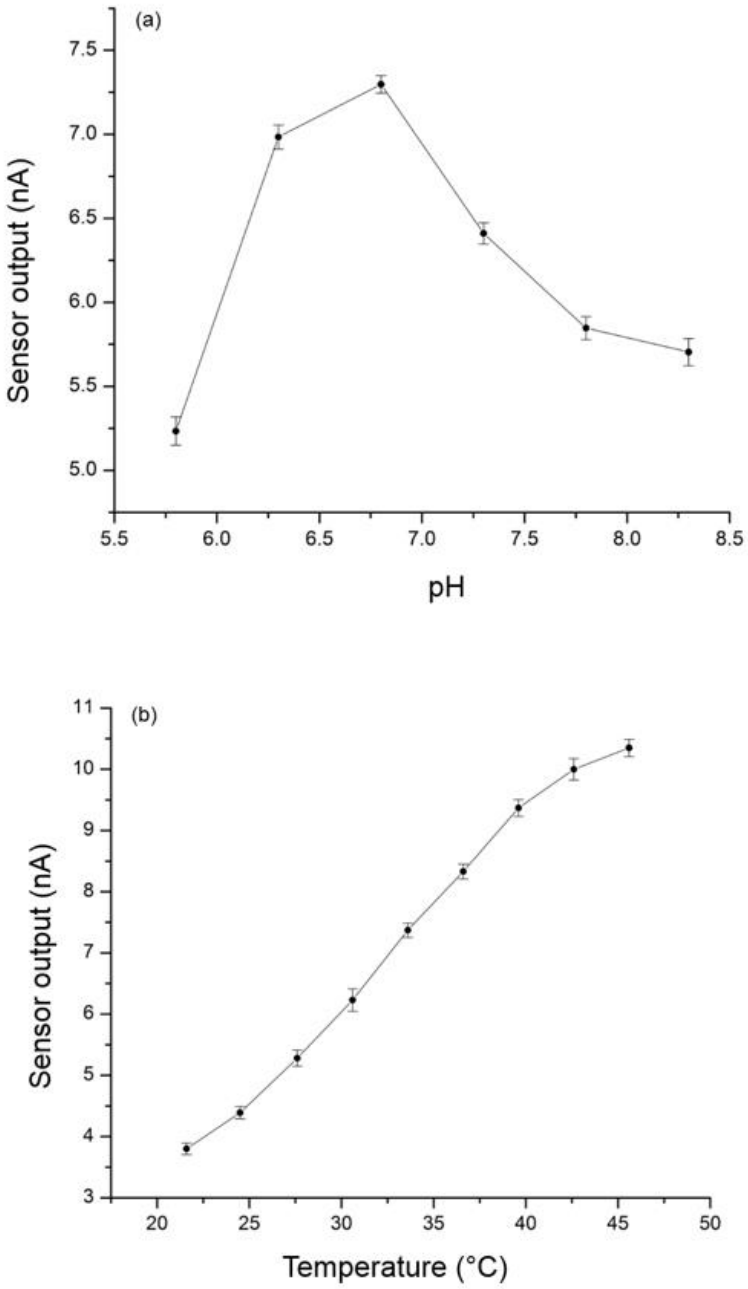

Fig. 4.5: (a) Effect of pH on the response of the uric acid biosensor in presence of 0.2 mM uric acid at 25˚C. (b) Effect of temperature on the response of uric acid biosensor in presence of 0.2 mM uric acid in 0.1 M PBS at pH 7. Error bar = ±S.D. and *n* = *3*.

We also tested the UA biosensor at various values of pH and temperature to evaluate their effects on the activity of the uricase enzyme. The pH-dependence of our sensor response was investigated in 0.2 mM uric acid solutions over a pH range of 5.8 to 8.3. The experimental results indicate that the sensor's output was dependent on pH of the solution and got the best response between pH 6.0 and 7.5 (Fig. 4.5a). Despite the fact that plasma pH does not change that much, our biosensor has the ability to keep its activity against pH decrements and increments. Since the pH values of a bird's blood and interstitial fluids are around 7.2 to 7.5, we can conclude that our sensor is likely to have good performance during *in-vivo* measurements [92]. The sensor's response in 0.2 mM uric acid solution was also tested between 22˚C and 45˚C. Since higher temperatures increase the activity of the enzyme and mass transport in surrounding solutions, higher sensor responses were generally obtained at higher temperatures (Fig. 4.5b). Temperature changes in bird's body will not cause notable changes in the enzyme activity. Even though temperature rises to high values, it will still be able to response effectively. Since the body temperatures of birds are generally around 40˚C [93], these results once again promise good prospects for *in-vivo* applications of this UA biosensor.

To test the sensor stability in storage, we measured sensor responses to 0.1 mM UA over a period of 3 weeks. Fully conditioned sensors were kept in 0.01 mM PBS (pH 7.4) at 4˚C while not in use. The UA sensor was able to keep 75% of its activity

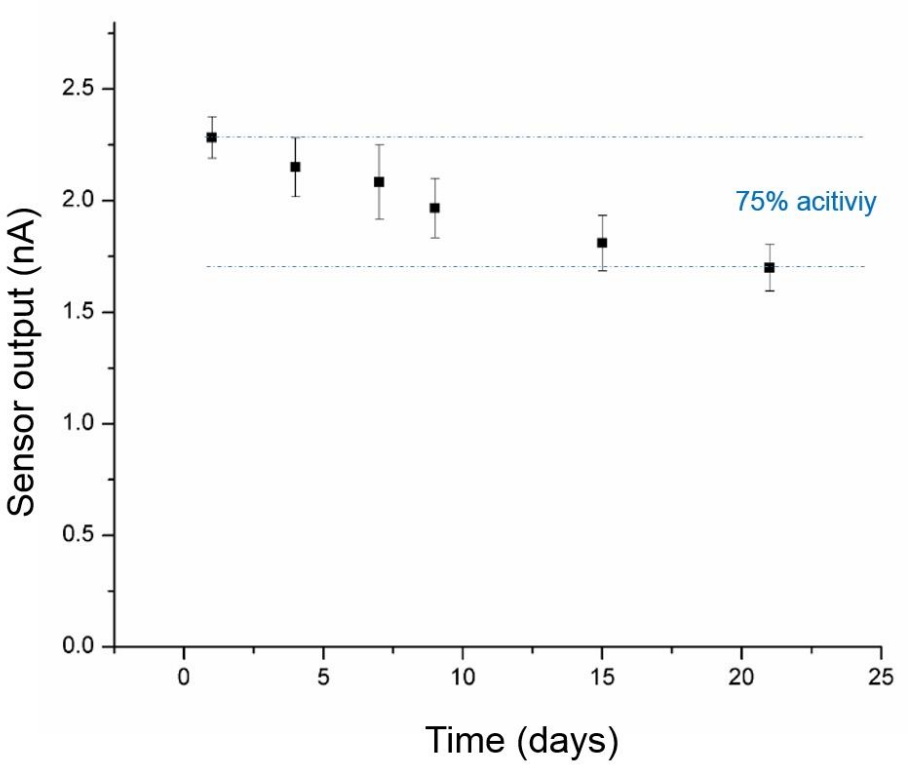

Fig. 4.6: Uric acid sensor storage stability. Sensor responses were measured for 0.1 mM uric acid. The sensor was kept in 0.01 mM PBS (pH 7.4) at 4˚C while not in use. Error bar = ±S.D. and n = 3.

after three weeks of storage, and the loss of activity was gradual over this period, with no indication of any threshold decays in performance (Fig. 4.6). After preparing the sensor, we can store the biosensor for 3 weeks. The reason for this response decrease could be deactivation of the uricase (UOx) enzyme or releasing of the UOx from the sensing layer over time.

To test operational stability, the sensor was stored in a 0.1M PBS solution at 37˚C, which contained 0.1 mM UA without any applied electrical potential. After a

week of storage, not significant change was observed in the sensor response. This indicates that this UA sensor could be used for continuous measurements of uric acid over a period of several days.

4.4.2 In-vivo measurements of extracellular uric acid levels in a domestic chicken

Although technological advances have been made in recent years for increasingly precise methods to measure uric acid levels in clinical and biological samples [76, 86, 94], this is apparently the first development of an *in-vivo* UA biosensor. Miniature needle-based sensors, with simple and robust fabrication procedures [60, 62], are good candidates for *in-vivo* sensing applications, and their structure makes them suitable for subcutaneous monitoring [68]. The needle-type *in-vivo* uric acid biosensor system developed here is really important to fulfill the need to understand the avian physiological states in real-time.

The sensing approach is based on real-time measurements in the interstitial fluid rather than a blood directly which helped the probe to be more free to move in response to movement of the bird without the worry of bleeding. The chicken fasted for 6 hours prior to the experiment to be able to decrease the uric acid levels 21. After inserting the biosensor system under the skin, sensor current stabilized within 10 minutes and the bird was then allowed to eat. No behavioral changes was observed in bird. The blood UA level was 0.1535 mM at the beginning of the experiment, and it reached 0.2511

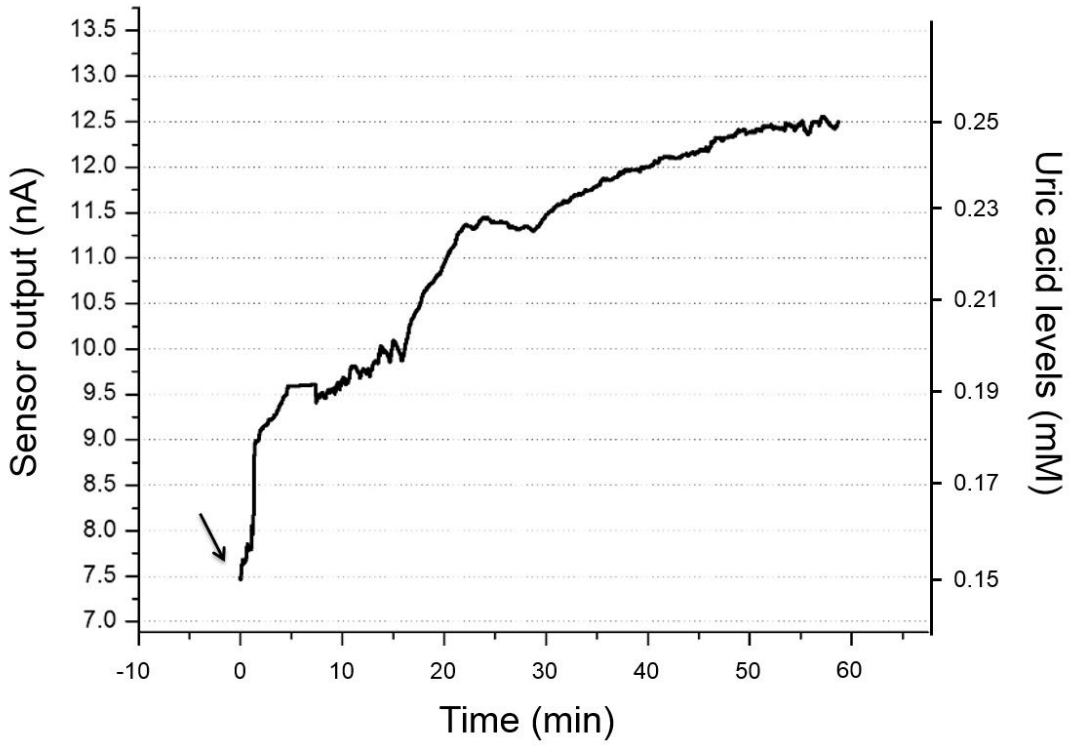

Fig. 4.7: In-vivo uric acid sensing. Sensor was placed subcutaneously under the skin and successfully detected uric acid level changes in domestic chicken. The arrow indicates where the bird was given access to feed.

mM (Fig. 4.7) at the end of the experiment. Not only the timing and size of the climb in uric acid biosensor output, but also having an inner membrane which prevents the effects of potentially interfering species, indicates that this climb was a consequence of feeding after fasting which effects the UA levels since it is the end product of protein catabolism in birds [72]. Our biosensor system was able to sense this UA level change in real-time successfully. The rapidly increasing uric acid levels demonstrate both that the sensor is sensitive and rapid-sensing and that uric acid levels in the interstitial fluid track those in blood closely. Through the experiment, it has been shown that the needle

type UA biosensor developed here can be used for in-vivo measurement of interstitial uric acid levels in birds. This is the first real time measurement of a blood chemical of a bird, which gives us an information about its physiological state. This study has a potential to open an innovative way to study of the physiological state of the avians.

4.5 Conclusions and Perspectives

In this work, we have developed a biosensor system that can continuously monitor *in-vivo* subcutaneous uric acid levels of birds in real-time. The uricase-based amperometric needle type biosensor developed here exhibits good performance in detecting uric acid at physiological levels with fast response time, good sensitivity, long-term stability and good resistivity against interfering chemical species. The results confirm a promising application of biosensors for *in-vivo* monitoring purposes of uric acid in birds. The impact of the study goes beyond the state-of-the-art uric acid sensors giving uric acid measurements in real-time. The system developed here could open up a new way of studying avian behavior which would lead to a better understanding of avian biology by enabling the integration of precise positional tracking data with a real-time dynamic measurement of the physiological state of the birds.

CHAPTER 5

LAB ON A BIRD: BIOPHYSICAL MONITORING OF FLYING BIRDS

5.1 Abstract

The metabolism of birds is finely tuned to their activities and environments, and thus research on avian systems can play an important role in understanding organismal responses to environmental changes. At present, however, the physiological monitoring of bird metabolism is limited by the inability to take real-time measurements of key metabolites during flight. In this study, we present an implantable biosensor system that can be used for continuous monitoring of uric acid levels of birds during various activities including flight. The system consists of a needle-type enzymatic biosensor for the amperometric detection of uric acid in interstitial fluids. A lightweight two-electrode potentiostat system drives the biosensor, reads the corresponding output current and wirelessly transfers the data or records to flash memory. We show how the device can be used to monitor, in real time, the effects of short-term flight and rest cycles on the uric acid levels of pigeons. In addition, we demonstrate that our device has the ability to measure uric acid level increase in homing pigeons while they fly freely. Successful application of the sensor in migratory birds could open up a new way of studying birds in flight which would lead to a better understanding of the ecology and biology of avian movements.

5.2 Introduction

Research on birds has served as an effective tool for ecological and evolutionary studies, as the metabolism of birds are finely tuned to their environments [12]. Development of new generations of radio-tags and data-loggers give the ability to track and study migratory birds by monitoring bird's dynamic locations [8, 58, 59]. Some transmitters can also give information from sensors that provide information about the bird's physiology such as heart rate and body temperature [95-97]. Continuous biophysical monitoring of birds, however, has been prevented by the absence of an autonomous sensor system that can make in vivo measurements on birds in flight. The current state-of-the-art for biophysical monitoring of birds is to take blood samples from the captured birds for their analysis in remote laboratories at later times [53-57]. This method only yields sporadic measurements of the birds' physiological state and is likely to be affected by the interrupted and disruptive sample-collection procedures.

Enzymatic needle-type in vivo biosensors have the potential for a more comprehensive and accurate analysis of physiological state by allowing continuous measurements in real time. Previously, enzymatic in vivo biosensor systems have been developed for measuring blood components such as glucose [60-62], cholesterol [63], and lactic acid [64-66]. Such sensors have also been used in animals for alcohol monitoring in Winstar rats [70], and glucose monitoring in fish [61]. Energy pathways in birds are dominated by lipid rather than carbohydrate metabolism, and somatic glucose level changes are not as informative as in mammalian system [71]. On the other

hand, uric acid is a good indicator of protein catabolism in birds since its presence in the body is a consequence of the breakdown of protein, either from catabolism of body protein or from recently digested proteinaceous food [72]. Birds primarily derive their energy from lipids, but some researchers have shown that there is an increase of the uric acid levels in birds undergoing short flights, which suggests that catabolism of body protein also occurs [98, 99]. Elevated uric acid levels after flying events have been observed in flying knots [98] and pigeons [100]. Our group has previously developed a needle-type enzymatic sensor system suitable for real-time amperometric monitoring of interstitial uric acid levels over the expected physiological range in domestic chickens [101]. In that work, besides characterizing the uric sensor performance *in vitro*, the effect of fasting and feeding events on the chickens' uric acid levels was successfully monitored in vivo with high sensitivity, thereby demonstrating the potential of the sensor system in studying avian systems. However, the significant weight and size of the device limited its use to non-flying chickens whose motions were greatly restricted.

We present here the Lab-on-a-Bird, an implantable lightweight biosensor system suitable for measurement of interstitial uric acid levels in flying birds in vivo. The system consists of a needle-type enzymatic biosensor for the amperometric detection of uric acid, and a two-electrode potentiostat system that drives the biosensor, reads the corresponding output current and wirelessly transfers the data or records to flash memory. In the following sections, we introduce the Lab-on-a-Bird and discuss

the preparation of its major components. We then demonstrate the application of the device in measuring uric acid levels in pigeons undergoing flights of varying durations.

5.3 Methods

5.3.1 System design and assembly

The Lab-on-a-Bird system shown in Fig. 5.1 and 5.2 consists of a needle-type biosensor for the amperometric detection of interstitial uric acid levels, and a two-electrode potentiostat system for driving the biosensor and collecting the data. Those two main components, along with a high capacity lithium polymer battery (3.7V, 40mA; Sparkfun Electronics, CO) are integrated inside a custom package. The entire system weighs approximately 6.5 g, which is well under 4% of an average pigeon's weight and allows for long-term tag-attachment without limiting their motion.

The lightweight two-electrode potentiostat system shown in Fig. 5.1b combines a low-power microcontroller ("MCU"; MSP430F2274 Texas Instruments, TX), a micro-power analog voltage reference (Intersil, CA), amplifiers (Maxim Integrated, CA), and filter blocks. The circuit drives the biosensor at 0.6 V through the low-power voltage reference and reads the corresponding ultra-low output current of the sensor (1 to 20 nA). A four-layer PCB board was designed and the circuit was built with a minimum number of components to decrease the weight of the total tag by keeping the circuit board area small. The potentiostat system is capable of recording the data to

internal flash memory or transmitting to a base station using an integrated CC2500 2.4 GHz wireless transceiver.

5.3.2 Uric acid biosensor preparation

The needle-type biosensor shown in Fig. 5.3a consists of two electrodes of platinum-iridium (Pt/Ir) wire and silver-silver chloride (Ag/AgCl) paste, and a sensing cavity on which uricase enzyme is immobilized. Detailed procedures for the biosensor fabrication and characterization are reported in our previous work [101]. Briefly, a Teflon coated Pt/Ir (10%) wire (0.125 mm o.d.; Advent Research Materials Ltd, Oxford, England) was stripped at one end to create a sensing cavity of 1 mm and the Ag wire (0.1 mm o.d.; Sigma Aldrich, St. Louis, MO) was wrapped around the Teflon coated surface. To create a reference/counter electrode, Ag/AgCl paste (CH Instruments Inc, USA) was applied onto the sensor body. To minimize the effects of interfering chemical species (e.g. ascorbic acid or glucose), the working electrode was coated with an inner membrane composed of Nafion and cellulose acetate. Prior to their in-vivo application, the uric acid sensors were characterized in vitro in a 1.5 mL cell that initially contained 0.1M PBS (pH 7.4) with saturated oxygen levels at room temperature (25 ˚C). The solutions of uric acid and/or interferents were injected into the cell and the corresponding sensor output was recorded for the calibration. The sensors were stored in 0.01 M PBS (pH 7.4) at 4 ˚C when not in use.

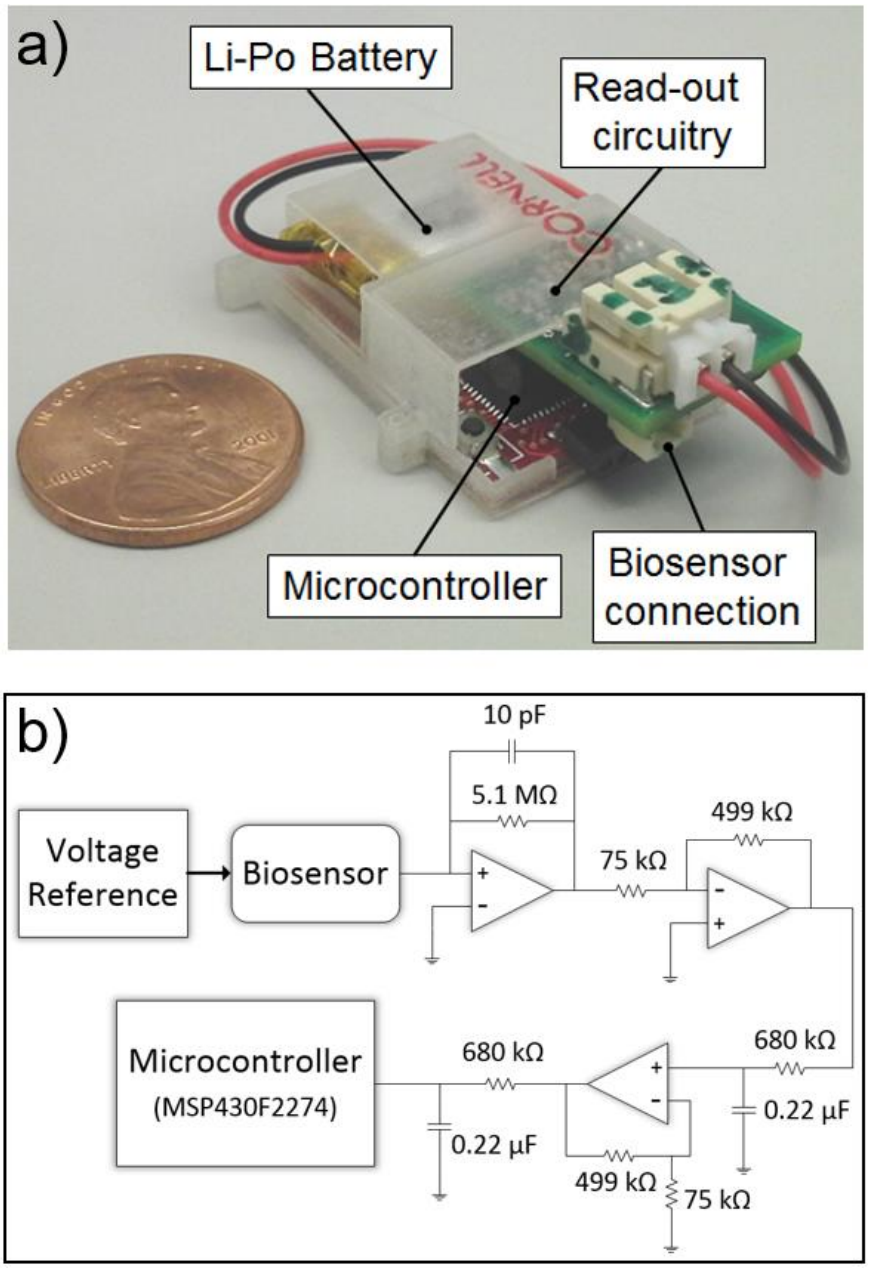

Fig. 5.1: a) The Lab-on-Bird system consisting of microcontroller, read-out circuitry, high capacity li-po battery and needle-type uric acid biosensor. b) Two-electrode potentiostat system for driving the biosensor and collecting the corresponding data.

Fig. 5.2: A pigeon with Lab-on-a-Bird system installed. The entire system weighs approximately 6.5 g, which is well under 4% of an average pigeon's weight and allows for long-term tag-attachment without limiting their motion.

5.3.3 In vivo sensor installation and calibration

The Lab-on-Bird system was implanted on the back of pigeons as shown in Fig. 5.2 and 5.3. In order to measure the uric acid levels in vivo, the needle type biosensor component of the Lab-on-a-Bird remained inside the subcutaneous tissue of the pigeons for interacting with the interstitial fluid. For the biosensor installation, a few feathers in the dorsal feather tract, anterior of the uropygial gland, were clipped at their bases

and the exposed skin was disinfected using Betadine antiseptic solution (Purdue Pharma, L.P., NJ). As shown in Fig. 5.3a, a 20-gauge catheter consisting of an outer polyurethane layer and an inner puncture needle (Terumo Medical Corporation, NJ) was inserted 1 cm subcutaneously. The inner puncture needle was then removed, and the outer layer of flexible polyurethane was cut just outside the skin surface. This created a cavity into which the needle type biosensor could be inserted. It and the surrounding remnant of the polyurethane catheter were secured to the skin with a ca. 2 cm X 4 cm piece of sterile Tegaderm® film (3M Corporate, MN). The custom packaging of the Lab-on-Bird system was attached on top of the sensor on the bird's back with a Rappole harness [89] made of dental floss or Stretch Magic© beading string. The harness ran around the bird's femurs and stably immobilized the Lab-on-a-Bird on the back of pigeons upon being fastened. Both the biosensor and battery were freely exchangeable, thus one Lab-on-a-Bird circuit could serve in multiple sensing applications with the exchange of fresh sensors and batteries. After installing the tag, we waited for 10 minutes for sensor current to stabilize.

Blood samples from pigeons were taken into heparinized blood collection tubes (Sarstedt CB-300) for biosensor calibration. For mid-range flying homing pigeon experiments, the blood samples were refrigerated immediately upon collection for further analysis in the lab. For short-term flying pigeon experiments, the blood samples were centrifuged at 6000 x g for ten minutes and then plasma was frozen at -86 °C. Uric acid concentration was measured using uric acid kit reagent sets (Teco

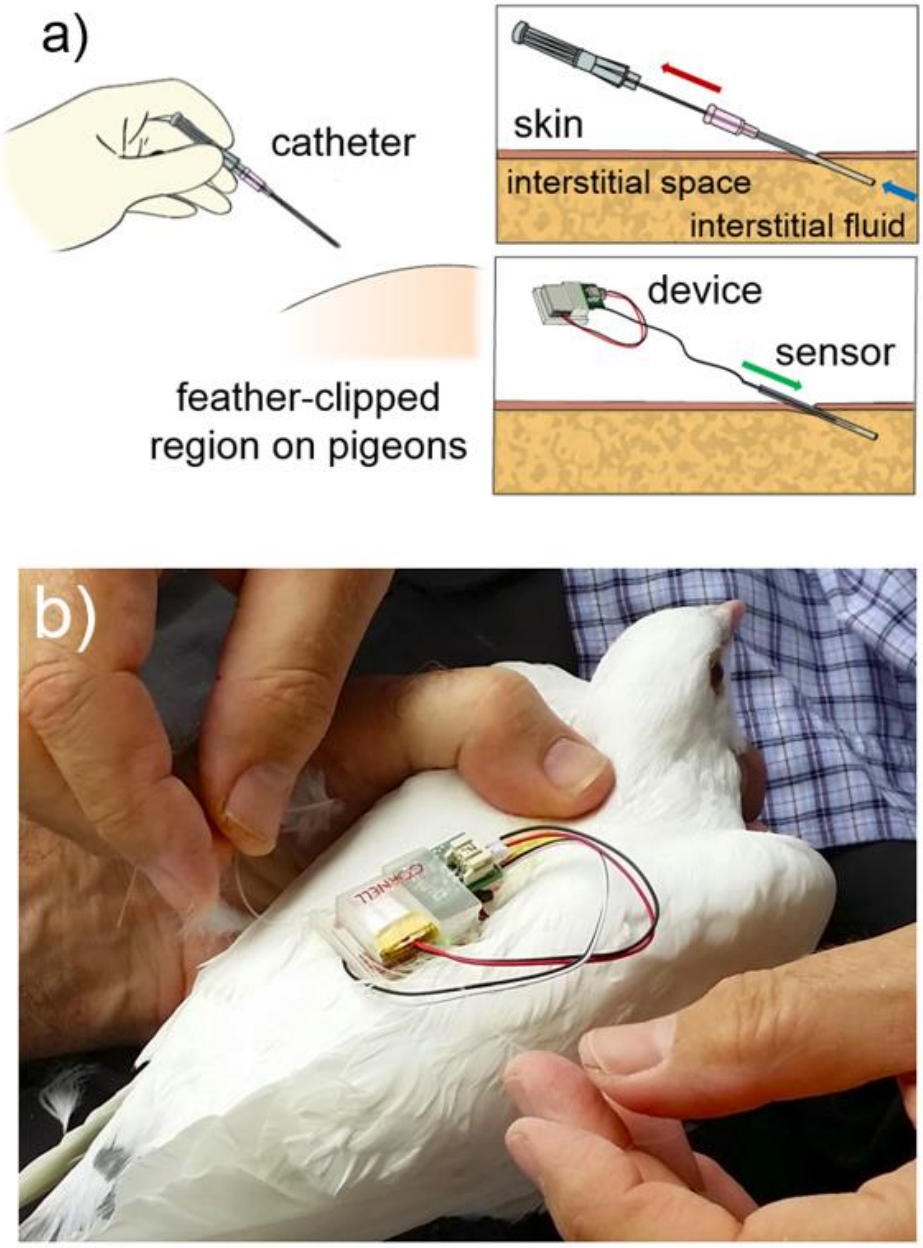

Fig. 5.3: a) Installation of the needle-type biosensor component of the Lab-on-a-Bird into the subcutaneous tissue of the pigeons for interacting with the interstitial fluid. b) A pigeon while installing the Lab-on-a-Bird system on the back of pigeon.

Diagnostics, CA or Wako Diagnostics, VA) and a spectrophotometer (Molecular Devices LLC, CA). Those uric acid levels were correlated to the biosensor output from the in vivo experiments using the one-point calibration method [102]. Here, the sensor sensitivity (S) is the ratio of the sensor output current (I), and the blood uric acid concentration (U). The uric acid concentration was estimated at any time from the sensor current I as $U(t) = I(t) / S$.

5.4 Results and Discussion

To evaluate the performance of the Lab-on-a-Bird system, we implanted the Lab-on-a-Bird on pigeons and used it to monitor changes in uric acid levels under two different flight conditions: short-range and mid-range flying. In order to see the effects of different intensities of exercise on the birds' uric acid levels and demonstrate the reversibility of the biosensor system, pigeons were studied under short-range flight and rest cycles in a constrained environment. Here we also examined the wearability of the Lab-on-a-Bird on flying birds. We then tested our device on homing pigeons for mid-range free flight experiments in the open sky to demonstrate the application of the Lab-on-a-Bird for longer term operations. All animal care procedures were approved by the Cornell University Institutional Animal Care and Use Committee (IACUC) with the

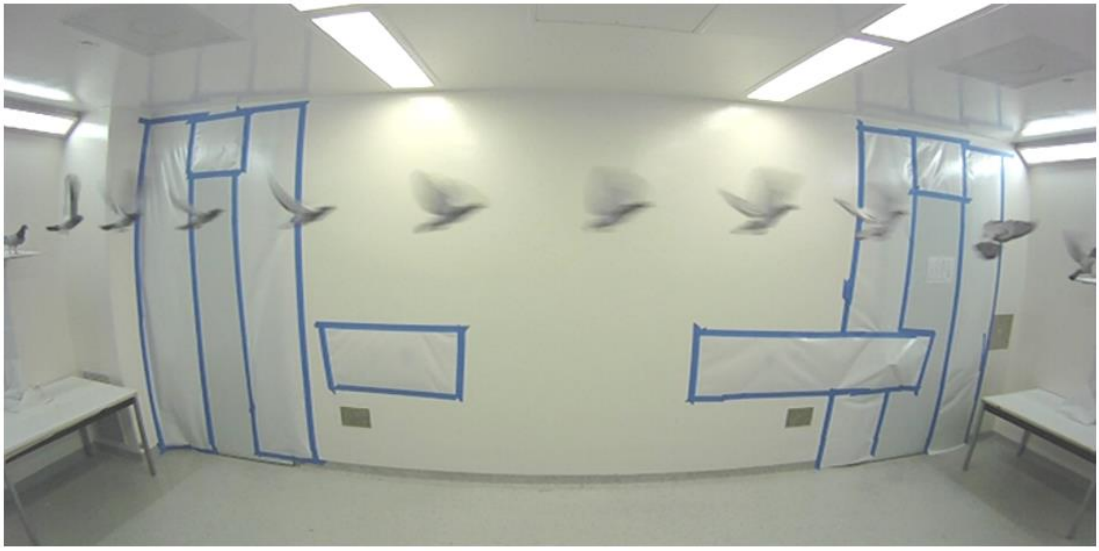

Fig. 5.4: Experimental setup for short-range flight experiments, a room with two platforms at opposite ends.

consultation of veterinarians from Cornell's Center for Animal Resources and Education and/or by the University of Western Ontario Animal Use Subcommittee.

5.4.1 Short-range flying pigeon experiments

As shown in Fig. 5.4, the short-range flight experiments were conducted in a room with two platforms at opposite ends. When released in the room, the pigeons would fly to one of these platforms and stand on them. With the approach of a researcher to that platform, accompanied by a click-note from the researcher, the trained pigeon would fly to the opposite platform on the other end and remain there until the next researcher approach. As a convention, we have designated one flight routine to be the pigeon's

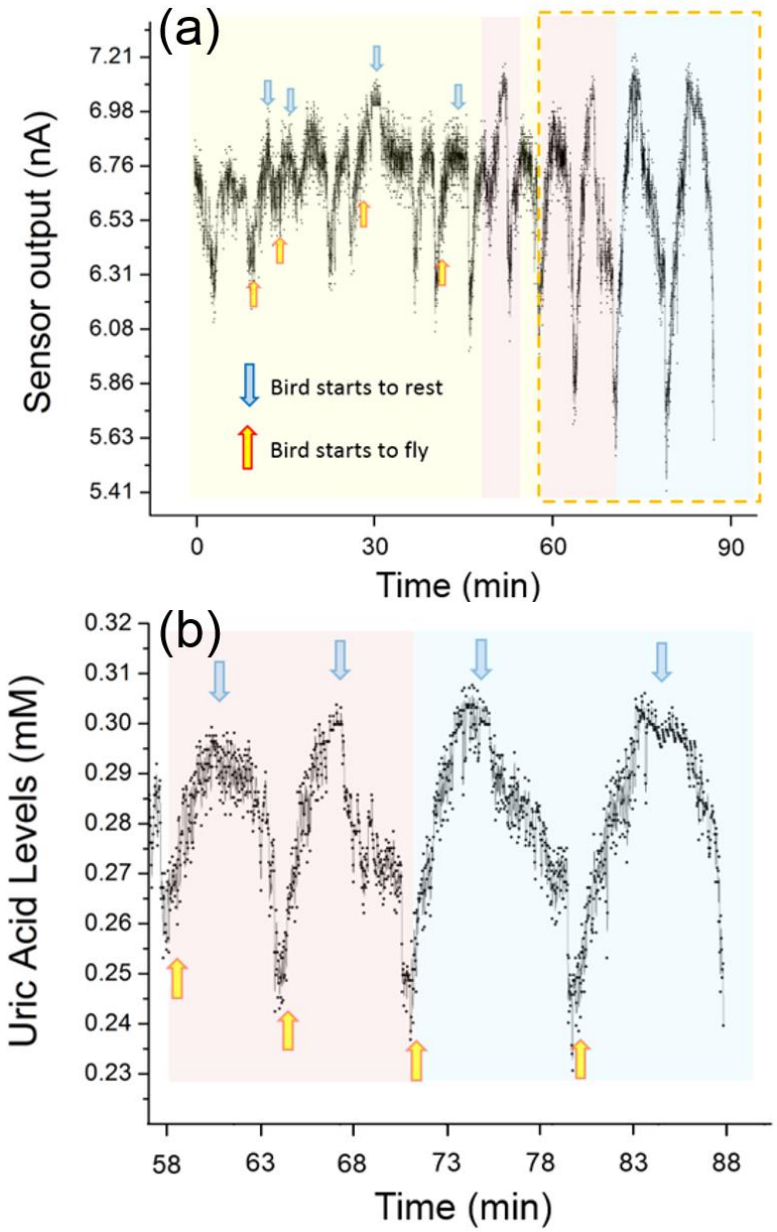

Fig. 5.5: a) Whole experiment data of short-range flight experiments. b) Last part of the experiment calibrated with the blood sample taken at the end of the experiment. Color codes represents as Yellow: 10 flight routines, Red: 20 flight routines, and Blue: 30 flight routines. Uric acid biosensor response increases when bird starts flight routines and decreases when rests.

flight to one platform and back to the original platform. We repeated this scheme for 10, 20 and 30 flight routines followed by resting periods. As described in more detail in our previous work [101], the interstitial uric acid is enzymatically reduced by the immobilized uricase enzyme of our needle-type sensor and converted into a measurable current output. Thus we expect that the biosensor output trends with the pigeon's interstitial uric acid levels. Here the sensor output was related to the uric acid levels by the one-point calibration using blood samples which we took immediately after the experimental flights.

There are three kinds of oxidative fuels in working muscles: carbohydrates, lipids, and proteins [103]. For endurance flights, fuel substrates are provided from sources outside the flight muscles such as adipose tissue [103]. Lipids stored in adipose tissue are the main fuel during long-term flights since it can deliver higher energy [98, 100]. On the other hand, for short-term flights, there are some constraints on fat mobilization and delivery, and therefore other fuel types can often be used [103]. Especially at take-off and during short flights, small muscular and hepatic carbohydrate stores are used [98]. We suggest that, for short-term flight routines, pigeons also use readily available proteins that have been stored in the muscle tissues. By keeping birds inactive after flight, they can adapt their metabolism to a new situation by reducing fat and protein utilization [71, 99]. As can be seen from Fig. 5.5a and 5.5b, the uric acid biosensor response increases when the pigeon starts its flight routines and decreases

while it rests. The pigeons may switch their energy usage mechanism depending on the distances of their travel.

5.4.2 Mid-range flying homing pigeon experiments

For the mid-range flying experiments, the Lab-on-a-Bird systems were installed on pigeons that were initially kept 30 miles away from their home and observed their uric acid level changes while they flew back home. Homing pigeons were trained one week before the actual experiment with dummy tags installed on them, which weighed around the same as the Lab-on-a-Bird devices (~ 6.5 g). This helped them get used to the tag and minimized the physiological alterations associated with their flying with foreign systems on the back. Before the releasing the pigeons, a blood sample was taken for determination of the uric acid levels. This data was then used for one-point calibration of the biosensor data. Biosensor read-outs were recorded to internal flash memory of the microcontroller in real-time while pigeons were flying.

Uric acid is a good indicator of protein catabolism in birds since its presence in the body is a consequence of the breakdown of protein, either from recently ingested proteinaceous food or from catabolism body protein [72]. We have previously demonstrated the sensing ability of needle-type biosensor system by collecting the *in vivo* extracellular uric acid measurements on a domestic chicken [101]. Uric acid levels increased after feeding the chicken with proteinaceous food and our biosensor was able to detect this change with fast response time and good sensitivity.

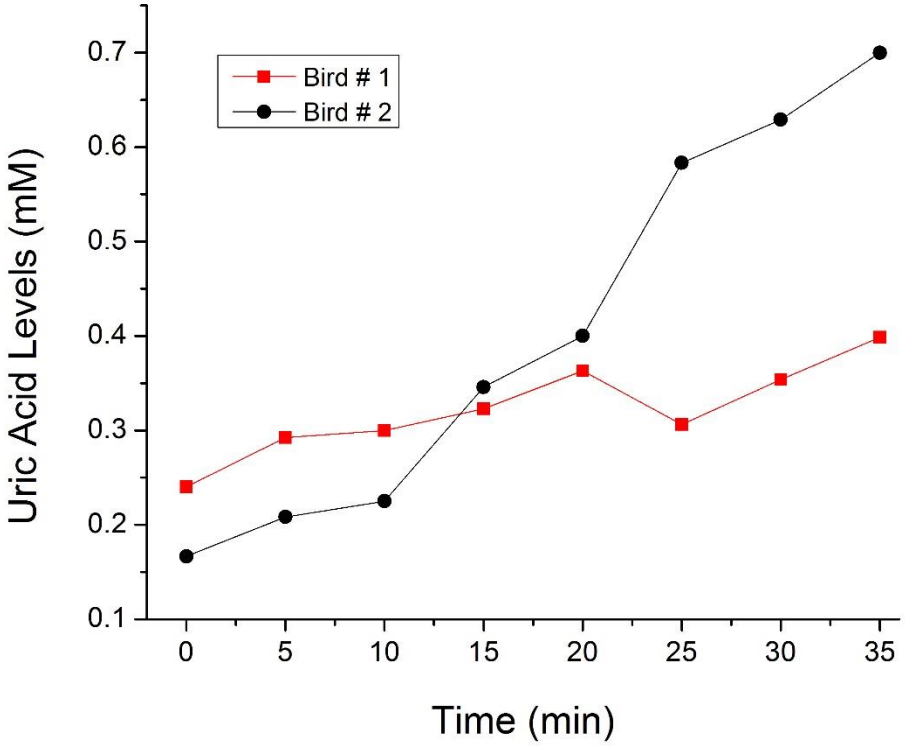

Fig. 5.6: Mid-range flight experiments. The Lab-on-a-Bird systems were installed on homing pigeons and uric acid level changes were observed while they flew back home.

Although birds primarily derive their energy from lipids, some researchers have shown that there is an increase of the uric acid levels in birds undergoing short flights, which suggests that catabolism of body protein also occurs.[98, 99] Elevated uric acid levels after flying events have been observed in flying knots[98] and pigeons[100]. As can be seen in Fig. 5.6, we have successfully observed this uric acid increase on homing pigeons during the first 35 minutes of the pigeon's flight back home. Even though there were no technical limitations for longer experimental trials

and measurements, the recording time of the tags was cut short when the birds flew into a rain-storm on the way back home. The prototype tags used in this experiment were not potted or coated to make them robust to rain. However, through the experiment, we have demonstrated that the needle type uric acid biosensor developed here can be used for in vivo measurement of interstitial uric acid levels in flying birds. Here for the first time, a biosensor system was installed on a flying bird to understand the relationship between energy consumption and real-time change in the uric acid levels while they fly.

5.5 Conclusions and Perspectives

In this work, we have developed the Lab-on-a-Bird, an implantable biosensor system which has the ability to measure uric acid levels in flying birds in vivo. We have successfully observed real-time changes in uric acid levels of flying pigeons. These are the first real-time measurements of a blood chemical of flying birds, which could be an indicator of their physiological states. These results confirm the promising application of the biosensor system for long term in vivo monitoring of birds, which could open a new way of studying birds in flight which would lead to a better understanding of the ecology and biology of avian systems. In the future, the Lab-on-a-Bird system can be further improved by multiplexing it for the detection of different analytes. Also by decreasing the weight of the system, smaller bird species could be studied.

CHAPTER 6

SMARTPHONE-ASSISTED SOLAR THERMAL POINT-OF-CARE DIAGNOSTIC DEVICE FOR CHOLERA DETECTION

6.1 Introduction

Vibrio Cholerae is a comma-shaped, gram negative bacterium which is the cause of an acute diarrheal disease in humans called “Cholera”. Infection can be caused by ingestion of contaminated food or water with the cholera bacterium which might cause death through extreme dehydration and electrolyte disturbances if left untreated. There are an estimated 3-5 million cholera cases over the world every year and 100,000-120,000 of them come to an end as deaths. Cholera has a relatively short incubation period varying between two hours to five days, which can potentially cause the rapid outbreaks [104].

Even though up to 80% of the cases can successfully be treated with oral rehydration salts, high death rates indicate that early and rapid detection of cholera is necessary to prevent spread of disease, increase the efficiency of treatments and decrease the intensity of epidemics. Traditional methods to identify V. Cholerae involving cultural, biochemical, and immunological assays are time-consuming and

laborious [105, 106]. There are commercially available rapid detection tests such as SMART™ test [107-110] and the Crystal VC® dipstick test [110-113], however they have sensitivity and specificity limitations [110, 111]. Point-of-care (POC) detection methods give us the ability to carry out the testing near the site of the patients without a need for hospitals and centralized laboratory-based environments. Advanced POC detection methods have been demonstrated for cholera detection, however these methods still need sample preparation steps consisting of centrifugation and some reagents that need to be refrigerated [114, 115]. There is a great need for a complete POC diagnostic device that can do all the sample preparation and detection steps in the field without the need for extensive laboratory equipment and an infrastructure-provided energy source.

Nucleic acid based detection methods such as the polymerase chain reaction (PCR) have been extensively developed for the diagnosis of genetic markers of diseases with high sensitivity and specificity [116, 117]. Miniaturization of these systems has led to the use of them for POC diagnostic applications with the goal of integration of sample processing, nucleic acid amplification, and detection systems in one package [118, 119]. There are examples of integration of all the analytical steps such as lysis, DNA extraction and purification on a single device [120-123]. Recently, researchers have also developed a solar thermal PCR system which removes the power requirements for thermal cycling, enabling a 100-fold reduction in power consumption [124].

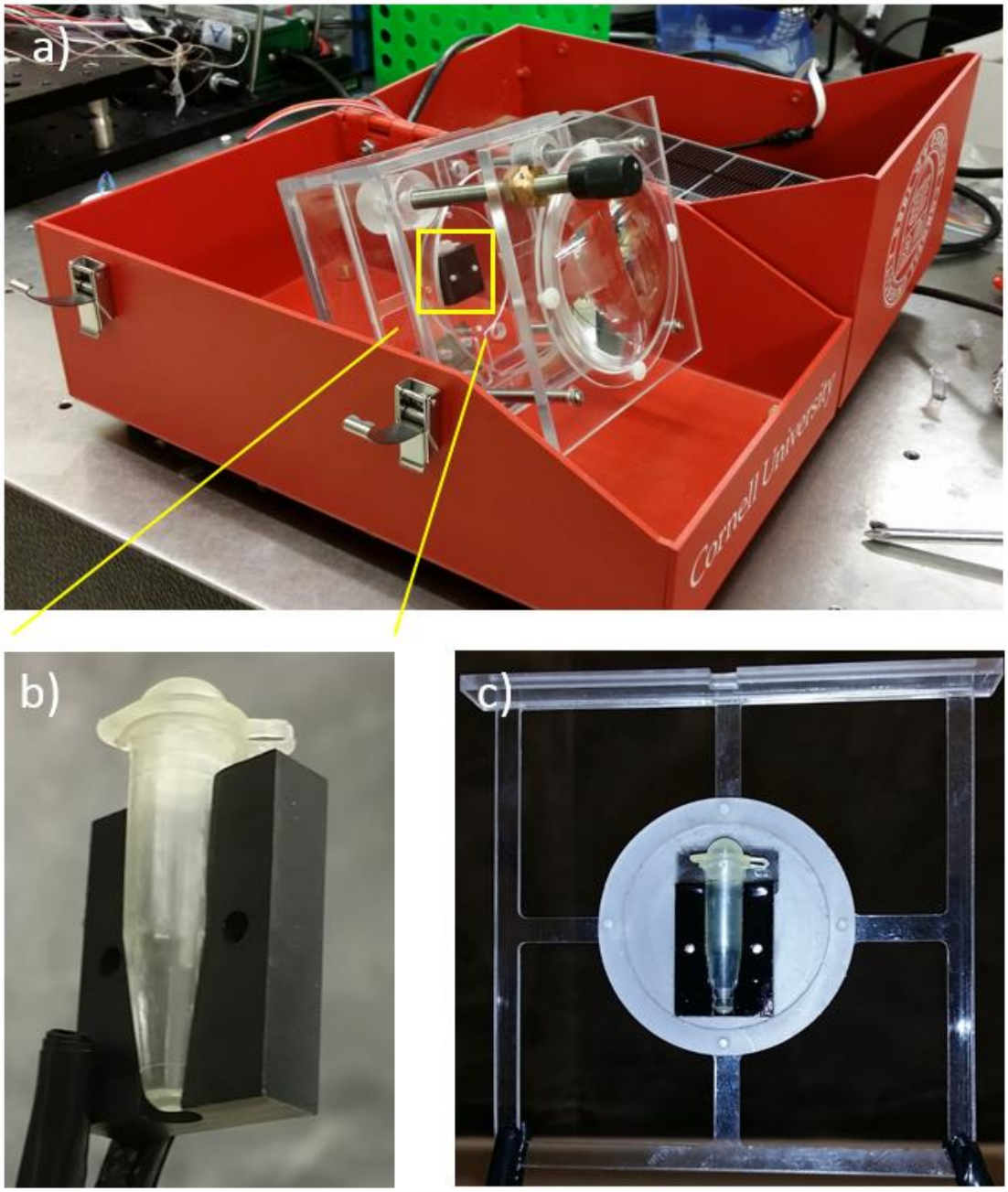

Fig. 6.1: Cholera-Detect system that introduces solar thermal DNA extraction method using solar-incubator which uses the sunlight to thermally lyse the bacteria to get the genetic information out of the cell.

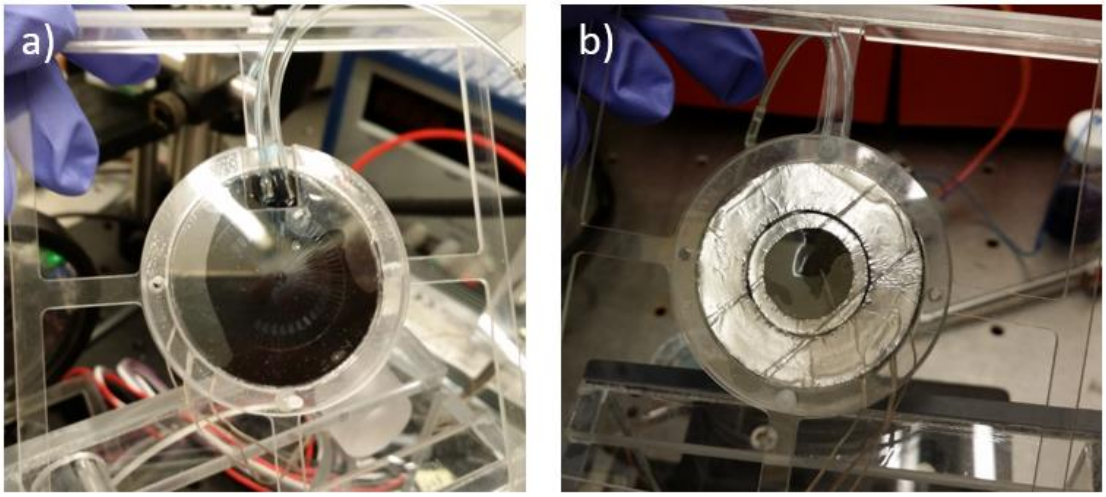

Fig. 6.2: Solar-PCR cartridge that fits into the interchangeable cartridge area of the Cholera-Detect system.

Even though there exist available on-chip assays for POC molecular diagnostics, pre-sample preparation steps such as target extraction and isolation have yet to be investigated sufficiently to be able to reach the ultimate goal for a POC genetic analysis device which has sample-in-answer-out capabilities [125]. Sample preparation is one of the most critical steps of POC assay developments for analytes present in complex matrices such as stool. High concentrations of interfering species (*e.g.*, proteins, enzymes) can be a problem at the detection step when working with real biological and clinical samples. To develop a fully integrated POC device, rapid and robust sample preparation techniques which don't need extensive laboratory equipment and reagents are necessary. Preparation of samples for downstream applications of diagnostic devices should be minimized and simplified, therefore making it more easily implemented in the field.

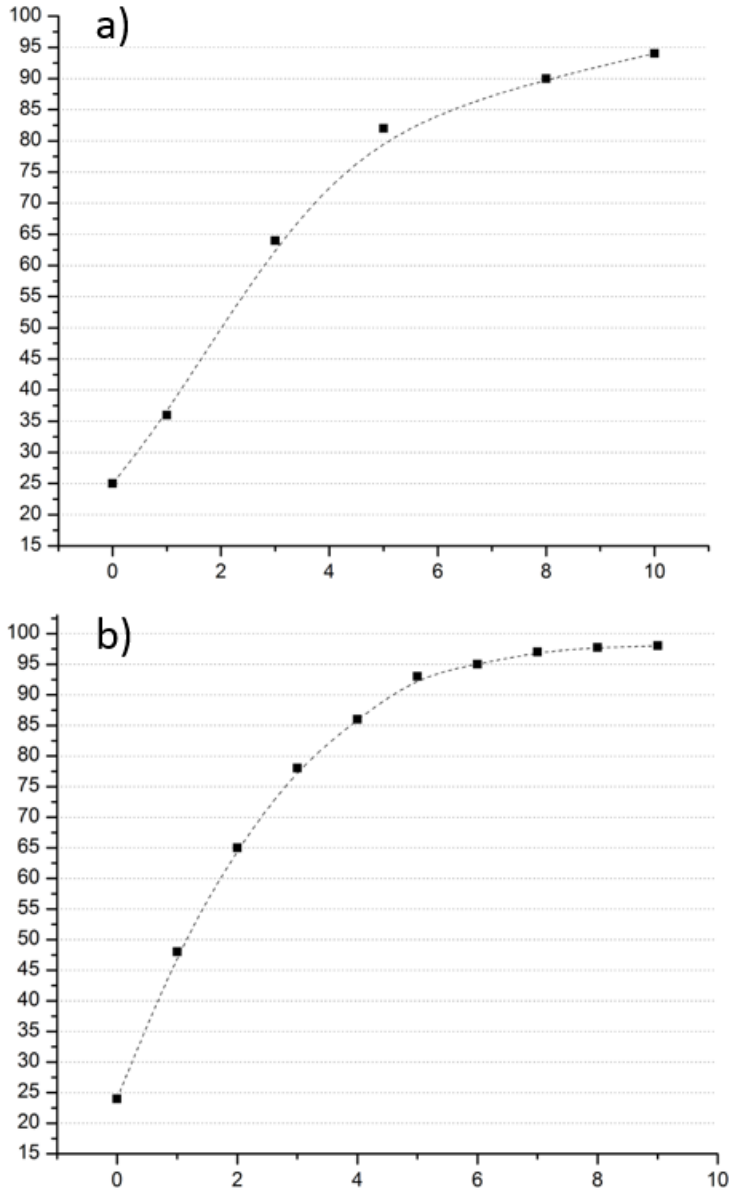

Fig. 6.3: Temperature measurements of the water inside the a) 0.5 mL b) 0.2 mL microcentrifuge tubes.

In this study, we have developed a Cholera-Detect system that introduces a solar thermal DNA extraction method using a solar-incubator, which uses the sunlight to thermally lyse the bacteria in order to extract the genetic information out of the cell. We have also used ChargeSwitch® magnetic microparticle-based technology to provide rapid and efficient DNA purification. We have then used isolated CTX DNA for downstream solar-PCR DNA amplification, previously developed by Jiang *et al.*, which combines solar heating with microfluidics to eliminate thermal cycling power requirements as well as create a simple device infrastructure for PCR. The Cholera-Detect system developed here has the ability to integrate simple DNA extraction and isolation capabilities from complex stool samples with solar-PCR amplification and smartphone assisted diagnosis of the results. We believe that exploiting the solar thermal energy as demonstrated here could give us the ability to carry out genetic analysis on the field without a need for hospitals and centralized laboratory-based environments.

6.2 Results and Discussion

6.2.1 Development and characterization of solar-incubator

The solar-incubator shown in Fig. 6.1 has the ability to lyse the bacteria thermally using sunlight and get the genetic information out of the cell. Black polycarbonate material was used as an absorber layer and also a holder for microcentrifuge tubes. Sunlight was focused using lenses and converted into heat by the absorber layer. A microcentrifuge

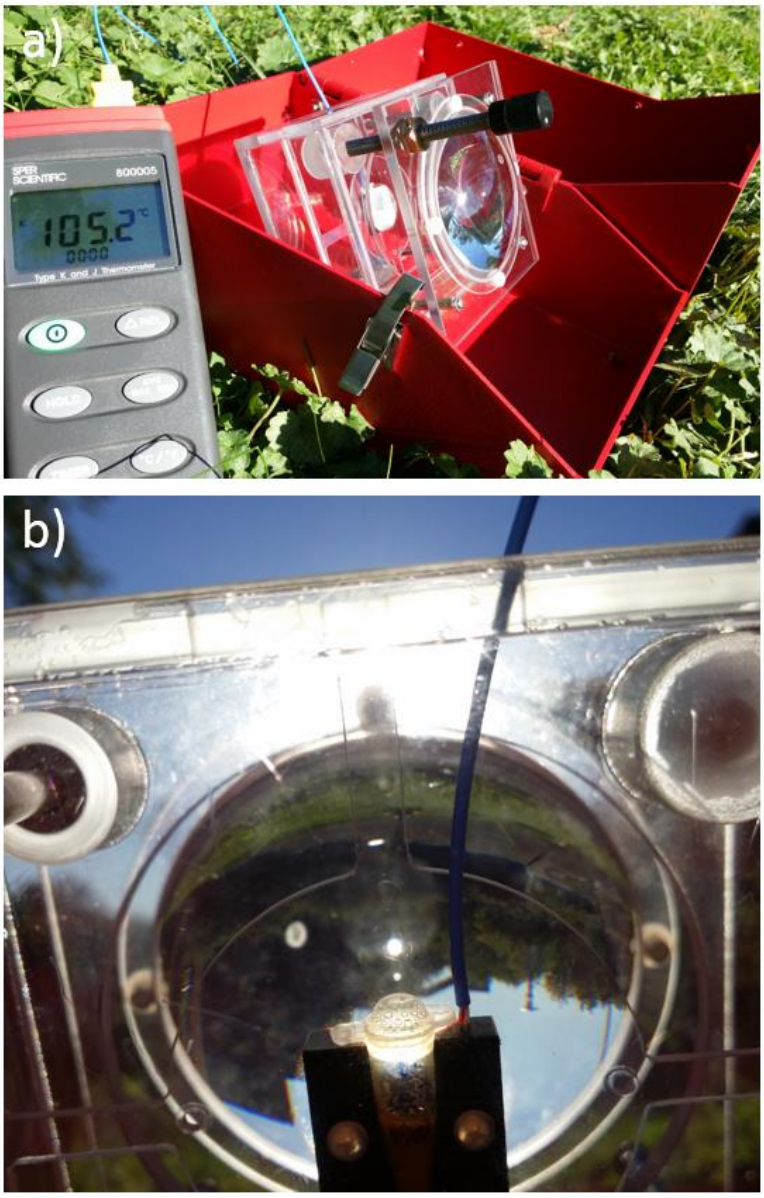

Fig. 6.4: a) Solar-incubator while operating at the outside where its temperature increases to 105 ˚C within 5 minutes after focusing sunlight. b) Temperature of the sample inside the microcentrifuge tube increases above 95 ˚C to realize the thermal lysing of the bacteria.

tube (0.5 mL or 0.2 mL) is attached to solar-incubator as shown in Fig. 6.1. The temperature of the liquid inside the tube can easily get up to 95 ˚C within 5 minutes (Fig. 6.3).

We have designed the solar-incubator from black polycarbonate thermo-plastic with high melting temperature (155 ˚C) which makes it a good material as an absorption layer. A drilled hole through solar incubator for 6 mm helped to measure its temperature using thermocouple which was then correlated with the solution temperature of the liquid inside microcentrifuge tube. Operation of the solar-incubator at the outside can be seen in Fig. 6.4 where its temperature increases to 105 ˚C within 5 min after focusing the sunlight. We have also analyzed the solar-incubator's temperature characteristics using COMSOL Multiphysics simulations. The heat transfer model includes black polycarbonate absorption layer, and polypropylene microcentrifuge with water inside. From simulations, we were able to see that polycarbonate material successfully distributes and delivers the heat absorbed from the sunlight and allow the liquid inside the microcentrifuge tube to heat up to desired lysing temperatures (Fig. 6.5 and Fig. 6.6).

6.2.2 Solar thermal PCR

Introducing sunlight to realize PCR reactions eliminates the energy burden for nucleic acid amplification while performing thermal cycling [124].

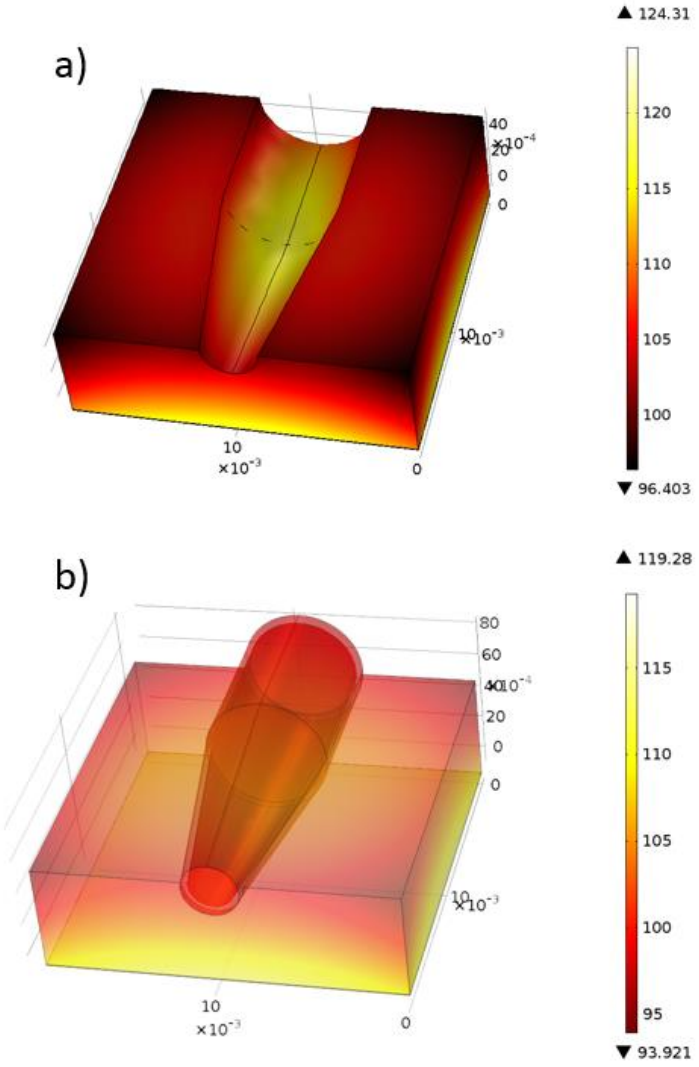

Fig. 6.5: Temperature simulations for solar-incubator. Polycarbonate material successfully distributes and delivers the heat absorbed from the sunlight. Temperature of the liquid inside the microcentrifuge tube to heat up to the desired lysing temperatures.

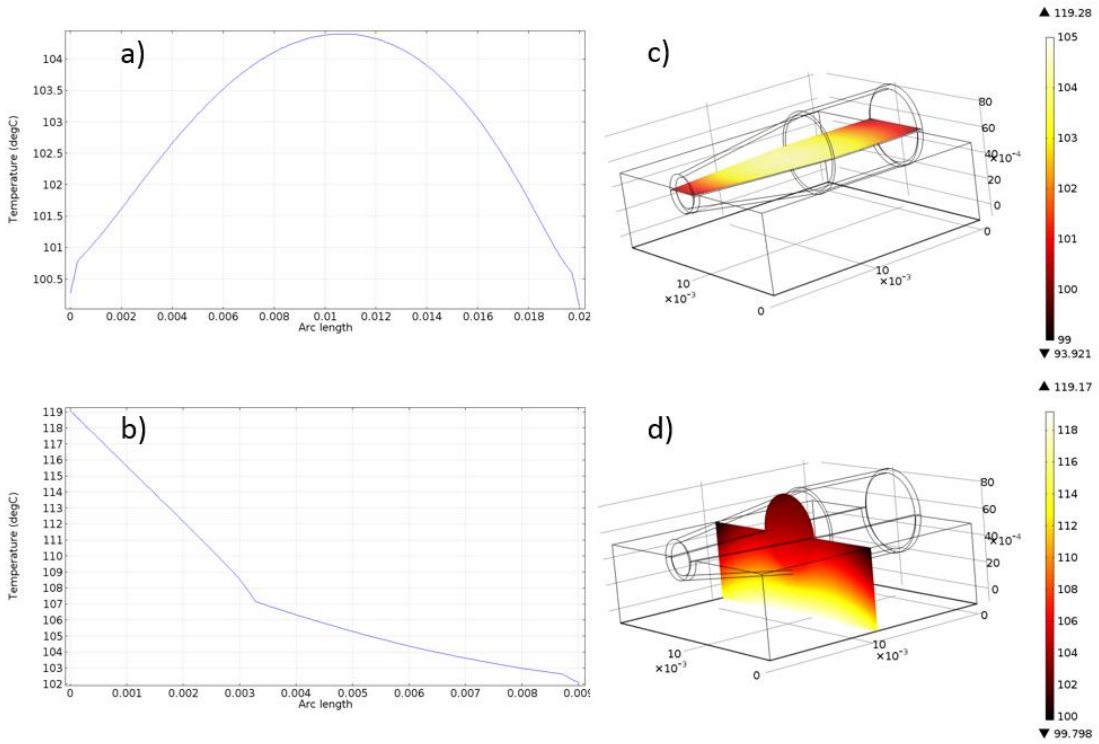

Fig. 6.6: Cross-sectional temperature distributions of solar incubator.

Fig. 6.2 shows solar-PCR cartridge that fits into the interchangeable cartridge area of the Cholera-Detect. Solar-PCR systems used here was previously developed in our laboratory to detect Kaposi Sarcoma [124]. A 75 mm diameter glass lens focuses light to the solar-PCR or solar incubator devices. Three thermocouples are inserted into the solar-PCR chips and one to the solar-incubator to measure the on-chip temperatures throughout the test by a custom smartphone app (Fig. 6.8). By changing the lens distance to the chips, desired temperatures can be achieved. Within the cholera genome, part of the DNA that codes for cholera toxin B was chosen as our target DNA. Specific

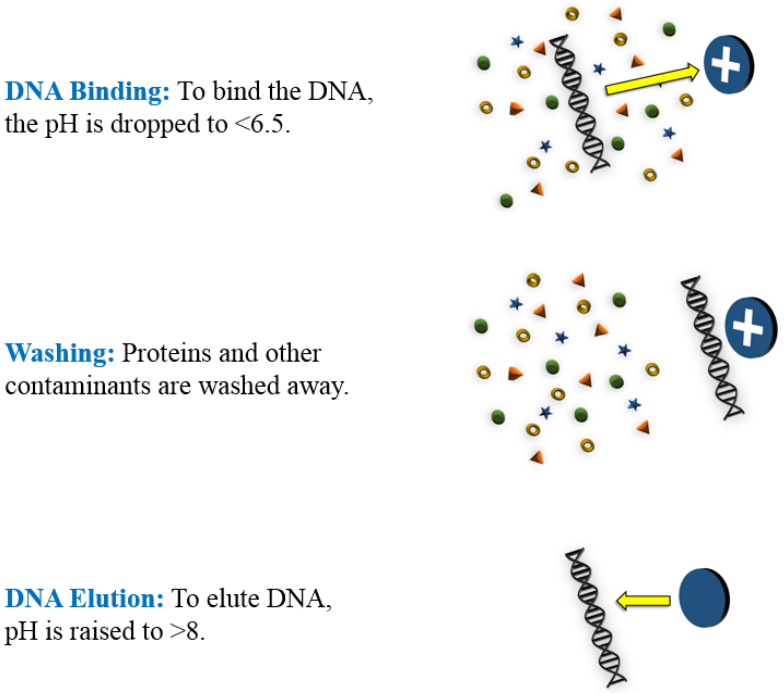

Fig. 6.7: Bacterial DNAs were isolated with the ChargeSwitch® gDNA Mini Bacteria Kit which uses magnetic microbead-based technology to provide rapid and efficient purification of DNA. Surface charge of the magnetic microbeads can be changed by altering the pH of the surrounding solution.

primers for this sequence were chosen using BLAST Primer Design, and ordered from Integrated DNA Technologies Inc. (Coralville, IA) (Table 6.1).

6.2.3 DNA extraction and isolation using sunlight and magnetic microparticles

Bacterial lysing is the first step for DNA analysis and involves releasing of the genomic materials and other cellular content by disassembling of the cellular membrane. Different lysing methods have been successfully demonstrated for POC applications

such as chemical lysis, thermal lysis, and lysing by mechanical forces or electrical pulses [126]. The advantage of thermal lysing is that no extra lysing reagents are needed that may interfere with downstream reactions and also may require refrigeration. Thermal lysing has been incorporated into microfluidic devices to perform on-chip lysis [127, 128] and some of them also include nucleic acid extraction capability which helps to isolate the nucleic acid from other cell components [129].

Isolation of nucleic acids is an important step since un-isolated samples may contain inhibitors that interfere with PCR or other target amplification processes [130]. Isolation can also help with target enrichment and increase the nucleic acid concentrations for sensitive detection [119]. DNA extraction and isolation in the same device for complex clinical samples like stool is still a remaining challenge for POC devices. Recently researchers have investigated minimal preparation needs for stool samples and their effect on cholera toxin detection results using microfluidic

Table 6.1: Probe and target sequences for cholera toxin B gene detection.

Name	Sequence
ctxB probe 1 (24 bp)	5'-CCACAACACACAAATACATACGCT-3'
ctxB probe 2 (24 bp)	5'-GGTATCCTTCATCCTTTCAATCGC-3'
ctxB target (178 bp)	CCACAACACACAAATACATACGCTAAATGATAAGATATTTTCGTATACAGAATCTCTAGCTGGAAAAAGAGAGATGGCTATCATTACTTTTAAGAATGGTGCAACTTTTCAAGTAGAAGTACCAGGTAGTCAACATATAGATTCACAAAAAAAAAGCGATTGAAAGGATGAAGGATACC

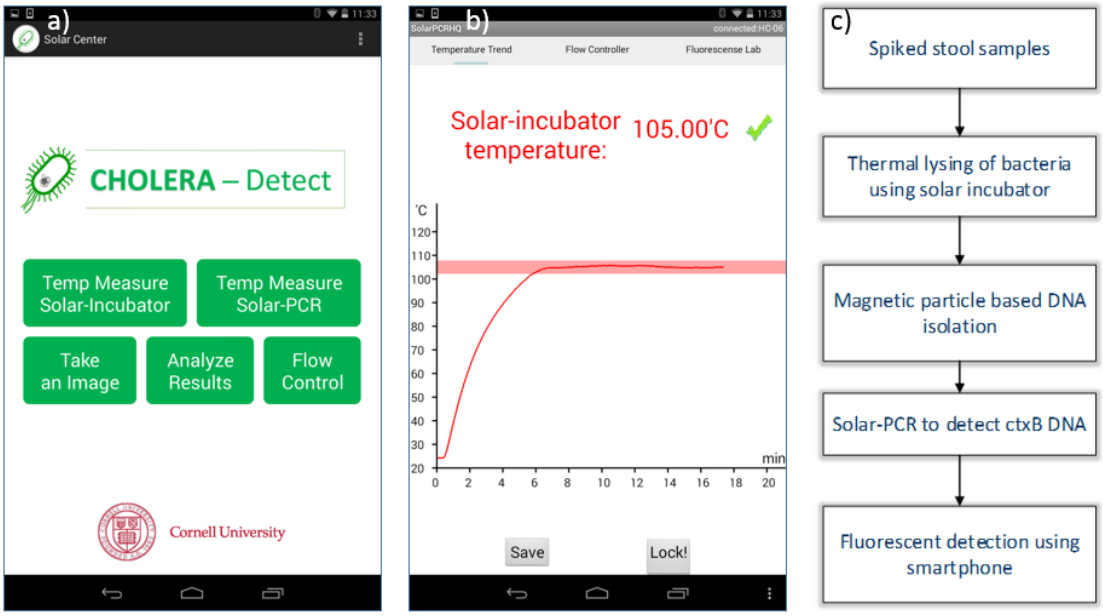

Fig. 6.8: Smartphone app and process flow for the Cholera-Detect system.

immunosensor [115]. However, sample preparation consisted of centrifugation or vacuum manifolds would not be appropriate for POC diagnostic applications where laboratory-based equipments are not reachable.

Here, we have developed a Cholera-Detect system that has 4 main components: First, a solar-incubator for lysing the bacteria thermally by using sunlight and extracting DNA out of the cell for further genetic analysis; second, a magnetic microparticle-based DNA isolation which uses ChargeSwitch® technology to provide rapid and

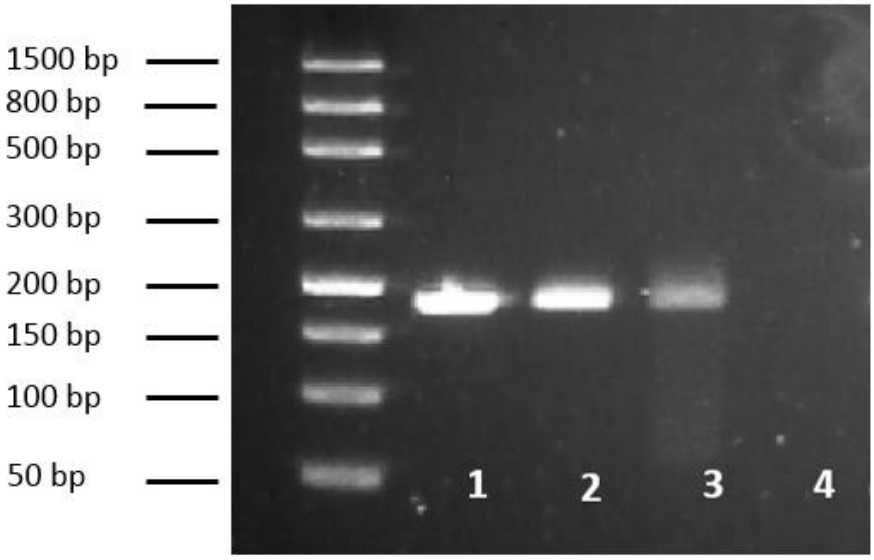

Fig. 6.9: Thermal cycler and solar-PCR amplification results. 1) and 2) are thermal cycler amplification. 3) CtxB DNA was successfully extracted and isolated from stool samples and amplified with solar-PCR. 4) Amplification of water (negative control).

efficient purification of DNA; third, solar-PCR based DNA amplification which uses the sunlight to realize PCR reaction which eliminates the energy burden for nucleic acid amplification while performing thermal cycling; and finally, smartphone assisting to the system for temperature measurements of the solar-incubator and solar-PCR devices, pump controls while PCR reactions and taking images of the results at the end and analyzing them to be able to do the diagnosis.

Fresh dog stool samples were collected from College of Veterinary Medicine, Cornell University, and stored at 4 ˚C when not in use in order to minimize the growth of the bacteria. After diluting the stool samples with 1X phosphate buffered saline (PBS) solution, they were spiked with fresh Escherichia coli (E. coli) HM109 bacterial

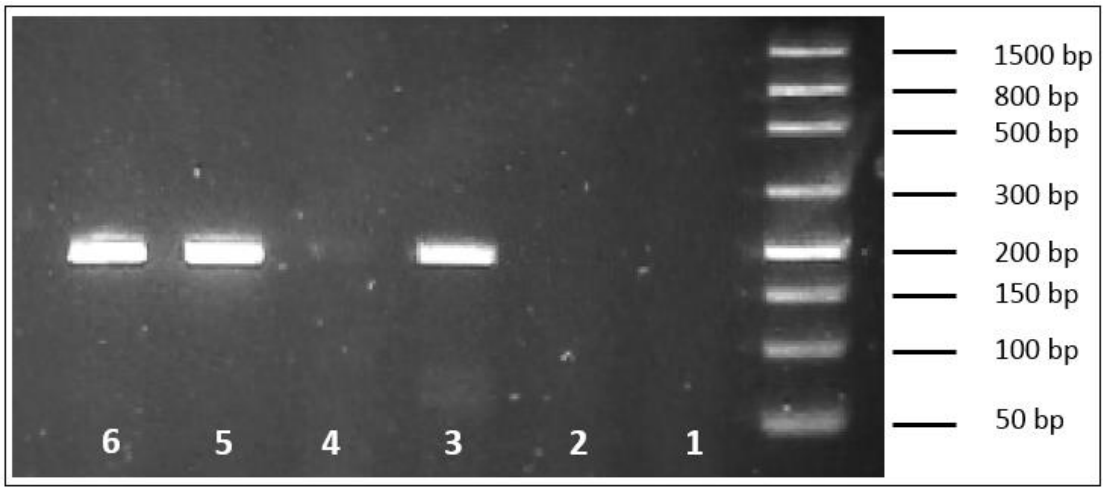

1 - Stool + ctxB bacteria (No Lysing) (No isolation)

2 - Stool + ctxB plasmid (LYSING)

3 - Stool + ctxB plasmid (LYSING) → DNA ISOLATION

4 - Stool + ctxB bacteria (LYSING)

5 - Stool + ctxB bacteria (LYSING) → DNA ISOLATION

6 - Stool + ctxB bacteria (LYSING) → DNA ISOLATION

Fig. 6.10: Amplification results where samples extracted and isolated with Cholera-Detect system. There were no results in the case of no-isolation because of the inhibitors inside the stool sample.

culture which were previous transformed with pIDTSMART-AMP:ctxB (plasmid with complete cholera toxin B gene, Table 6.1) plasmid to get bacterial numbers around $10x10^6$ CFU/ml. Spiked stool samples were used for the experiments directly. To achieve bacterial lysing, 150 µL of spiked stool sample was transferred into 0.2 mL microcentrifuge tube and thermally lysed for 10 minutes at around 95 ˚C. Bacterial DNAs were then isolated with the ChargeSwitch® gDNA Mini Bacteria Kit which uses magnetic microbead-based technology to provide rapid and efficient purification of

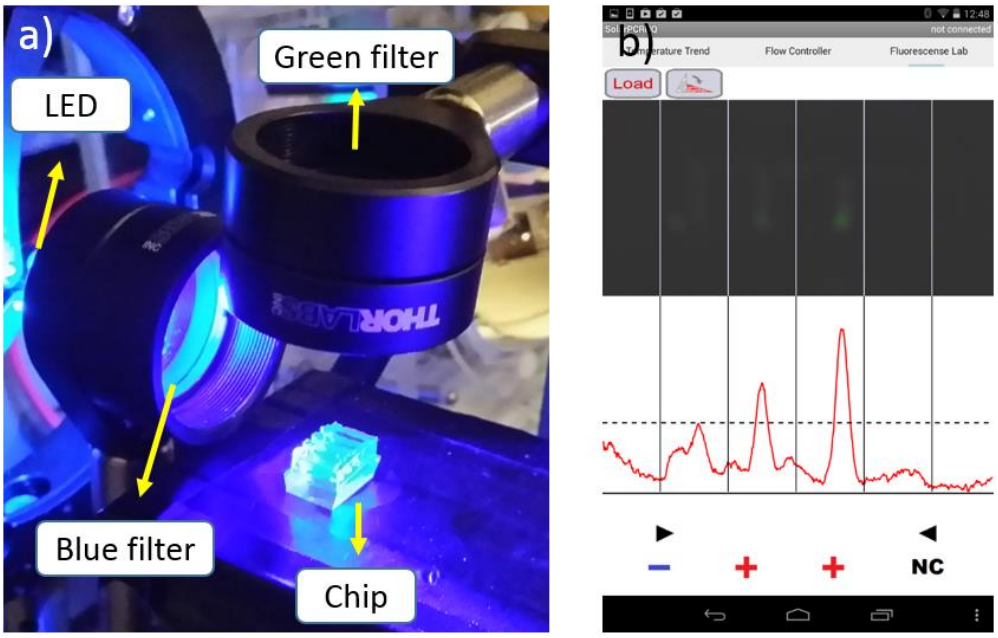

Fig. 6.11: Smartphone-based fluorescent detection setup. Images were taken and analyzed using smartphone.

DNA. Magnetic microbeads are coated with an ionizable functional group whose affinity for nucleic acids is pH dependent, in order to facilitate nucleic acid isolation without the need for hazardous chemicals, centrifugation, or vacuum manifolds. Lysed stool samples are mixed with 15 µL magnetic microbeads with binding solution (pH < 6.0) to bind the DNA to magnetic microbeads. After incubating at room temperature for 1 min, beads were collected with small magnet for 1 min until the beads formed a tight pellet. After removing the supernatant, 250 µL wash buffer was added, (pH = 7.0) and mixed gently. Beads were again collected with the magnet for 1 minute, and supernatant were removed. To be able to elute the DNA from beads, eluting buffer (pH = 8.5) was added and mixed gently. To increase the elution efficiency, the solution was

incubated at 60 ˚C for 5 minutes using solar incubator. Then beads were collected with magnet again and supernatant containing DNA was transferred to a clean microcentrifuge tube for PCR amplification reactions. For characterization experiments, a solar simulator setup was used which consists of a 100 W white LED lamp and lens, a cooling fan, an aluminum heat sink and 2 extra light collimation lenses. We used a regular thermal cycler to analyze the results to characterize the system. We have also successfully amplified the extracted and isolated samples using solar-PCR (Fig. 6.9). A Flashgel Electrophoresis system was used to analyze the amplified DNA. As can be seen from the results in Fig. 6.10, we were able to successfully extract and isolate DNA from both *ctxB* plasmid, and transformed *E.coli* spiked stool using the Cholera-Detect system, where we obtained no results if there was no isolation probably because of the inhibitors inside the stool sample. Smartphone-based fluorescent detection setup was used to take and analyze the images of the amplified nucleic acids (Fig. 6.11).

6.3 Conclusions and Perspectives

The study presented here focused on the application of solar thermal power for bacterial DNA extraction, isolation and amplification in stool samples for POC molecular diagnosis applications. The solar-incubator is a great tool for thermal lysing of bacteria, with the ability to heat up to 95 ˚C within 5 minutes. The Cholera-Detect system developed here gives us the ability to do rapid and on field molecular diagnosis of

cholera without the need for extensive laboratory equipments, chemicals and an infrastructure-provided energy source which would potentially make it possible to improve health care in outbreak situations.

CHAPTER 7

CONCLUSIONS AND DISCUSSIONS

In the first part, we have investigated a conducting polymer device that achieves a continuum of microenvironments for cell growth to affect the migration behaviour of bovine aortic endothelial cells. Marked differences were observed as a function of location along the polymer stripe, and a 3-fold variation is achieved in cell migration speed and directional persistence time. Directional cell migration along the conducting polymer stripe was induced. A gradient in adsorbed fibronectin indicates that a spatial variation in cell adhesion is at play. Compared to other techniques that are used to control cell behaviour, the device discussed here offers the advantages of simplicity and electrical control, and might yield a useful tool for cell biology. Migration can be slowed down or accelerated, enabling the study of the signal transduction mechanisms governing cell speed, extension, sensing and directionality. Because these are the same cell behaviours critical to multiple biological processes, including cancer cell metastasis, inflammatory response, wound healing and embryonic development, implementing such a device could lead to the identification and study of molecular targets mediating these processes. In the future, actively switchable pixelated microdevices can be implemented to control cell behaviors more precisely.

In the second part, we have developed a real-time in vivo uric acid biosensor system, Lab-on-a-Bird, for biophysical monitoring of birds. The metabolism of birds is finely tuned to their activities and environments, and thus research on avian systems can play an important role in understanding organismal responses to environmental changes and ecological investigations. After characterization of the sensor system, we demonstrated the autonomous operation of the system by collecting in vivo extracellular uric acid measurements on a domestic chicken. We then show how the device can be used to monitor, in real time, the effects of short-term flight and rest cycles on the uric acid levels of pigeons. In addition, we demonstrate that our device has the ability to measure uric acid level increase in homing pigeons while they fly freely to back home. Successful application of the sensor in migratory birds could open up a new way of studying birds in flight which would lead to a better understanding of the ecology and biology of avian movements. Lab-on-a-Bird system can be further improved by multiplexing the detection capability for different analytes. Also by decreasing the weight of the system, smaller bird species can be studied.

Finally, we have presented a Cholera-Detect system for point-of-care detection of Vibrio Cholerae which is a comma-shaped, gram negative bacterium and the cause of an acute diarrhoeal disease in humans called “Cholera”. Even though up to 80% of the cases can be successfully treated with oral rehydration salts, around 100,000 – 120,000 of the cases come to an end as deaths. This indicates that early and rapid detection of the cholera is necessary to prevent spread of disease, increase the

efficiency of treatments and decrease the intensity of epidemics. Cholera-Detect system developed here has the ability to do rapid, and on-field molecular diagnosis of cholera without need for extensive laboratory equipment and chemicals which would potentially make possible improved health care in outbreak situations. The main advantage of the Cholera-Detect system is to exploit the sunlight for nucleic acid extraction, isolation and amplification which eliminates the need for some of the required equipments and chemicals. Cholera-Detect systems capability can easily be extended to detect other diseases by changing the molecular markers. Solar thermal power can also be used for other molecular diagnosis techniques such as isothermal amplification of DNA.

BIBLIOGRAPHY

[1] I. Willner, and E. Katz, *Bioelectronics: From Theory to Applications*, Weinheim: Wiley-VCH Verlag GmbH & Co. KGaA, 2005.

[2] A. Bozkurt, R. F. Gilmour, and A. Lal, "Balloon-assisted flight of radio-controlled insect biobots," *Biomedical Engineering, IEEE Transactions on*, vol. 56, no. 9, pp. 2304-2307, 2009.

[3] D. Erickson, D. O'Dell, L. Jiang *et al.*, "Smartphone technology can be transformative to the deployment of lab-on-chip diagnostics," *Lab on a chip*, 2014.

[4] E. Meng, and R. Sheybani, "Insight: implantable medical devices," *Lab on a Chip*, 2014.

[5] D. M. Taylor, S. I. H. Tillery, and A. B. Schwartz, "Direct cortical control of 3D neuroprosthetic devices," *Science*, vol. 296, no. 5574, pp. 1829-1832, 2002.

[6] M. Velliste, S. Perel, M. C. Spalding *et al.*, "Cortical control of a prosthetic arm for self-feeding," *Nature*, vol. 453, no. 7198, pp. 1098-1101, 2008.

[7] M. S. Bowlin, and M. Wikelski, "Pointed wings, low wingloading and calm air reduce migratory flight costs in songbirds," *PLoS One*, vol. 3, no. 5, pp. e2154, 2008.

[8] W. D. Robinson, M. S. Bowlin, I. Bisson *et al.*, "Integrating concepts and technologies to advance the study of bird migration," *Front Ecol Environ*, vol. 8, pp. 354-361, 2010.

[9] L. R. Hochberg, D. Bacher, B. Jarosiewicz *et al.*, "Reach and grasp by people with tetraplegia using a neurally controlled robotic arm," *Nature*, vol. 485, no. 7398, pp. 372-375, 2012.

[10] A. Bozkurt, R. F. Gilmour, A. Sinha *et al.*, "Insect–machine interface based neurocybernetics," *Biomedical Engineering, IEEE Transactions on,* vol. 56, no. 6, pp. 1727-1733, 2009.

[11] A. J. Chung, B. Cordovez, N. Jasuja *et al.*, "Implantable microfluidic and electronic systems for insect flight manipulation," *Microfluidics and nanofluidics,* vol. 13, no. 2, pp. 345-352, 2012.

[12] L. J. Wright, R. A. Hoblyn, R. E. Green *et al.*, "Importance of climatic and environmental change in the demography of a multi-brooded passerine, the woodlard Lullula arborea," *Journal of Animal Ecology,* vol. 78, pp. 1191-1202, 2009.

[13] A. Darwish, and A. E. Hassanien, "Wearable and implantable wireless sensor network solutions for healthcare monitoring," *Sensors,* vol. 11, no. 6, pp. 5561-5595, 2011.

[14] M. Berggren, and A. Richter-Dahlfors, "Organic bioelectronics," *Advanced Materials,* vol. 19, pp. 3201-3213, 2007.

[15] D. Khodagholy, T. Doublet, P. Quilichini *et al.*, "In vivo recordings of brain activity using organic transistors," *Nature communications,* vol. 4, pp. 1575, 2013.

[16] A. Gumus, J. P. Califano, A. M. Wan *et al.*, "Control of cell migration using a conducting polymer device," *Soft Matter,* vol. 6, no. 20, pp. 5138-5142, 2010.

[17] A. M. D. Wan, D. J. Brooks, A. Gumus *et al.*, "Electrical control of cell density gradients on a conducting polymer surface," *Chem Comm,* vol. 35, pp. 5278-5280, 2009.

[18] R. M. Owens, and G. G. Malliaras, "Organic electronics at the interface with biology," *MRS bulletin,* vol. 35, no. 06, pp. 449-456, 2010.

[19] J. Rivnay, R. M. Owens, and G. G. Malliaras, "The rise of organic bioelectronics," *Chemistry of Materials,* vol. 26, no. 1, pp. 679-685, 2013.

[20] D. A. Lauffenburger, and A. F. Horwitz, "Cell migration: a physical integrated molecular process," *Cell,* vol. 84, pp. 359-369, 1996.

[21] G. Chan, and D. J. Mooney, "New materials for tissue engineering: towards greater control over the biological response," *Trends in Biotechnology,* vol. 26, pp. 382-392, 2008.

[22] B. K. Brandley, and R. L. Schnaar, "Tumor cell haptotaxis on covalently immobilized linear and exponential gradients of a cell adhesion peptide," *Developmental Biology,* vol. 135, pp. 74-86, 1989.

[23] S. A. DeLong, J. J. Moon, and J. L. West, "Covalently immobilized gradients of bFGF on hydrogel scaffolds for directed cell migration," *Biomaterials,* vol. 26, pp. 3227-3234, 2005.

[24] C. Lo, H. Wang, M. Dembo *et al.*, "Cell movement is guided by the rigidity of the substrate," *Biophysical Journal,* vol. 79, pp. 144-152, 2000.

[25] S. R. Peyton, C. M. Ghajar, C. B. Khatiwala *et al.*, "The emergence of ECM mechanics and cytoskeletal tension as important regulators of cell function," *Cell Biochem Biophys,* vol. 47, pp. 300-320, 2007.

[26] A. Curtis, and C. Wilkinson, "Topographical control of cells," *Biomaterials,* vol. 18, pp. 1573-1583, 1997.

[27] G. Malliaras, and R. Friend, "An organic electronics primer," *Phys. Today,* vol. 58, pp. 53-58, 2005.

[28] D. H. Kim, S. Richardson-Burns, L. Povlich *et al.*, *Indwelling neural implants: strategies for contending with the in vivo environment,* p.^pp. 165-207, Boca Raton, FL: CRC Press, Taylor and Francis, 2010.

[29] D. T. Simon, S. Kurup, K. C. Larsson *et al.*, "Organic electronics for precise delivery of neurotransmitters to modulate mammalian sensory function," *Nature Materials,* vol. 8, pp. 742-746, 2009.

[30] J. Isaksson, P. Kjall, D. Nilsson *et al.*, "Electronic control of Ca 2+ signalling in neuronal cells using an organic electronic ion pump," *Nature Materials,* vol. 6, pp. 673-679, 2007.

[31] J. Isaksson, C. Tengstedt, M. Fahlman *et al.*, "A solid-state organic electronic wettability switch," *Advanced Materials,* vol. 16, pp. 316-320, 2004.

[32] J. Y. Wong, R. Langer, and D. E. Ingber, "Electrically conducting polymers can noninvasively control the shape and growth of mammalian cells," *PNAS,* vol. 91, pp. 3201-3204, 1994.

[33] C. Salto, E. Saindon, M. Bolin *et al.*, "Control of neural stem cell adhesion and density by an electronic polymer surface switch," *Langmuir,* vol. 24, pp. 14133-14138, 2008.

[34] J. C. Gustaffson, B. Liedberg, and O. Inganas, "In situ spectroscopic investigations of electrochromism and ion transport in a poly (3,4-ethylenedioxythiophene) electrode in a solid state electrochemical cell," *Solid State Ionics,* vol. 69, pp. 145-152, 1994.

[35] H. G. Othmer, S. R. Dunbar, and W. Alt, "Models of dispersal in biological systems," *Journal of mathematical biology,* vol. 26, no. 3, pp. 263-298, 1988.

[36] Y. L. Hu, S. Li, H. Miao *et al.*, "Roles of microtubule dynamics and small GTPase rac in endothelial cell migration and lamellipodium formation under flow," *JOURNAL OF VASCULAR RESEARCH,* vol. 39, no. 6, pp. 465-476, 2002.

[37] L. Liu, B. D. Ratner, E. H. Sage *et al.*, "Endothelial cell migration on surface-density gradients of fibronectin, VEGF, or both proteins," *Langmuir : the ACS journal of surfaces and colloids,* vol. 23, no. 22, pp. 11168-11173, 2007.

[38] X. Lin, and B. P. Helmke, "Micropatterned structural control suppresses mechanotaxis of endothelial cells," *Biophysical journal,* vol. 95, no. 6, pp. 3066-3078, 2008.

[39] P. A. DiMilla, K. Barbee, and D. A. Lauffenburger, “Mathematical model for the effects of adhesion and mechanics on cell migration speed,” *Biophysical Journal*, vol. 60, no. 1, pp. 15-37, 1991.

[40] S. P. Palecek, J. C. Loftus, M. H. Ginsberg *et al.*, “Integrin-ligand binding properties govern cell migration speed through cell-substratum adhesiveness,” *Nature*, vol. 385, no. 6616, pp. 537-540, 1997.

[41] J. T. Smith, J. K. Tomfohr, M. C. Wells *et al.*, “Measurement of cell migration on surface-bound fibronectin gradients,” *Langmuir : the ACS journal of surfaces and colloids*, vol. 20, no. 19, pp. 8279-8286, 2004.

[42] S. B. Carter, “Effects of Cytochalasins on Mammalian Cells,” *Nature*, vol. 213, no. 5073, pp. 261-264, 1967.

[43] J. T. Mabeck, J. A. DeFranco, D. A. Bernards *et al.*, “Microfluidic gating of an organic electrochemical transistor,” *Applied Physics Letters*, vol. 87, no. 1, pp. 013503-013503-3, 2005.

[44] S. Y. Yang, J. A. Defranco, Y. A. Sylvester *et al.*, “Integration of a surface-directed microfluidic system with an organic electrochemical transistor array for multi-analyte biosensors,” *Lab on a chip*, vol. 9, no. 5, pp. 704-708, 2009.

[45] D. J. Pennisi, and T. Mikawa, "Normal patterning of the coronary capillary plexus is dependent on the correct transmural gradient of FGF expression in the myocardium," Generic, Elsevier, 2005.

[46] C. M. Nelson, W. F. Liu, and C. S. Chen, *Methods in Molecular Biology*, p.^pp. 1-9, Berlin: Springer, 2005.

[47] M. M. Rosenkilde, and T. W. Schwartz, “The chemokine system–a major regulator of angiogenesis in health and disease,” *Apmis*, vol. 112, no. 7-8, pp. 481-495, 2004.

[48] C.-L. E. Helm, M. E. Fleury, and A. H. Zisch, “Synergy between interstitial flow and VEGF directs capillary morphogenesis in vitro through a gradient amplification mechanism,” *Proceedings of the National Academy of Sciences*

of the United States of America [H.W. Wilson - GS], vol. 102, no. 44, pp. 15779, 2005.

[49] S.-Y. Cheng, S. Heilman, M. Wasserman *et al.*, "A hydrogel-based microfluidic device for the studies of directed cell migration," *Lab on a chip,* vol. 7, no. 6, pp. 763-769, 2007.

[50] C. E. Schmidt, V. R. Shastri, J. P. Vacanti *et al.*, "Stimulation of neurite outgrowth using an electrically conducting polymer," *Proceedings of the National Academy of Sciences of the United States of America,* vol. 94, no. 17, pp. 8948-8953, 1997.

[51] B. Winther-Jensen, and K. West, "Vapor-phase polymerization of 3,4-ethylenedioxythiophene: A route to highly conducting polymer surface layers," *MACROMOLECULES,* vol. 37, no. 12, pp. 4538-4543, 2004.

[52] K. M. Yamada, K. Olden, and I. Pastan, "Transformation-sensitive cell surface protein: isolation, characterization, and role in cellular morphology and adhesion," *Annals of the New York Academy of Sciences,* vol. 312, pp. 256, 1978.

[53] M. Hau, S. A. Gill, and W. Goymann, "Tropical field endocrinology: Ecology and evolution of testosterone concentrations in male birds.," *General and Comparative Endocrinology,* vol. 157, no. 3, pp. 241-248, 2008.

[54] S. Jenni-Eiermann, L. Jenni, and T. Piersma, "Plasma metabolites reflect seasonally changing metabolic processes in a long-distance migrant shorebird (Calidris canutus), ," *Zoology,* vol. 105, no. 3, pp. 239-246, 2002.

[55] M. Kern, W. Bacon, D. Long *et al.*, "Blood metabolite and corticosterone levels in breeding adult Pied Flycatchers.," *Condor,* vol. 107, no. 3, pp. 655-667, 2005.

[56] M. D. Kern, W. Bacon, D. Long *et al.*, "Blood metabolite levels in normal and handicapped pied flycatchers rearing broods of different sizes.," *Comparative Biochemistry and Physiology a-Molecular & Integrative Physiology,* vol. 147, no. 1, pp. 70-76, 2007.

[57] H. Wada, I. T. Moore, C. W. Breuner *et al.*, "Stress responses in tropical sparrows: Comparing tropical and temperate Zonotrichia.," *Physiological and Biochemical Zoology, ,* vol. 79, no. 4, pp. 784-792, 2006.

[58] R. MacCurdy, R. Gabrielson, E. Spaulding *et al.*, "Automatic animal tracking using matched filters and time difference of arrival," *Journal of Communications,* vol. 4, pp. 487-495, 2009.

[59] L. J. Wilson, A. C. McSorley, Gray M. C. *et al.*, "Radio-telemetry as a tool to define protected areas for seabirds in the marine environment," *Biological Conservation,* vol. 142, pp. 1808-1817, 2009.

[60] D. Bindra, Y. Zhang, and G. Wilson, "Design and in Vitro Studies of a Needle-Type Glucose Sensor for Subcutaneous Monitoring," *Anal. Chem. ,* vol. 63, pp. 1692-1696, 1991.

[61] Y. Endo, K. Yonemori, H. F. Hibi *et al.*, "Wireless enzyme sensor system for real-time monitoring of blood glucose levels in fish. ," *Biosensors and Bioelectronics,* vol. 24, pp. 1417-1423, 2009.

[62] Y. Hu, and G. Wilson, "Rapid Changes in Local Extracellular Rat Brain Glucose Observed with an In Vivo Glucose Sensor," *Journal of Neurochemistry* vol. 68, pp. 1745-1752, 1997.

[63] Y. Yonemori, Y. Yonemori, M. Murata *et al.*, "Wireless biosensor system for real-time cholesterol monitoring in fish "Nila tilapia"," *Talanta,* vol. 80, pp. 909-915, 2009.

[64] A. Guiseppie-Elie, "An implantable biochip to influence patient outcomes following trauma-induced hemorrhage," *Anal Bioanal Chem,* vol. 399, pp. 403-419, 2011.

[65] Y. Hu, Y. Zhang, and G. Wilson, "A needle-type enzyme-based lactate sensor for in vivo monitoring," *Analytica Chimica Acta,* vol. 281, pp. 503-511, 1993.

[66] S. Suman, R. Singhal, A. Sharma *et al.*, "Development of a lactate biosensor based on conducting copolymer bound lactate oxidase," *Sensors and Actuators B,* vol. 107, pp. 768-772, 2005.

[67] J. J. Mastrototaro, "The MiniMed continuous glucose monitoring system," *Diabetes Technology*, vol. 2, pp. 13-18, 2000.

[68] C. Choleau, J. C. Klein, G. Reach *et al.*, "Calibration of a subcutaneous amperometric glucose sensor Part 1. Effect of measurement uncertainties on the determination of sensor sensitivity and background current," *Biosensors and Bioelectronics,* vol. 17, pp. 641-646, 2002.

[69] J. Wang, "Electrochemical glucose biosensors," *Chem. Rev.,* vol. 108, pp. 814-825, 2008.

[70] C. P. Cheney, B. Srijanto, D. L. Hadden *et al.*, "In vivo wireless ethanol vapor detection in the Wistar rat," *Sensors and Actuators B,* vol. 138, pp. 264-269, 2009.

[71] M. M. Landys, T. Piersma, C. G. Guglielmo *et al.*, "Metabolic profile of long-distance migratory flight and stopover in a shorebird," *Proceedings of the Royal Society B-Biological Sciences,* vol. 272, no. 1560, pp. 295-302, 2005.

[72] R. J. Johnson, Y. Y. Sautin, W. J. Oliver *et al.*, "Lessons from comparative physiology: could uric acid represents a physiological alarm signal gone awry in western society?," *J Comp Physiol B,* vol. 179, no. 67-76, 2009.

[73] Y. Lv, Z. Zhang, and F. Chen, "Chemiluminescence biosensor chip based on a microreactor using carrier air flow for the determination of uric acid in human serum," *The Analyst,* vol. 127, pp. 1176-1179, 2002.

[74] D. Rocha, and F. Rocha, ". A flow-based procedure with solenoid micro-pumps for the spectrophotometric determination of uric acid in urine," *Microchemical Journal,* vol. 94, pp. 53-59, 2010.

[75] D. Martinez-Perez, M. L. Ferrer, and C. R. Mateo, "A reagent less fluorescent sol-gel biosensor for uric acid detection in biological fluids," *Analytical Biochemistry,* vol. 322, pp. 238-242, 2003.

[76] K. Jindal, M. Tomar, and V. Gupta, "CuO thin film based uric acid biosensor enhanced response characteristics.," *Biosensors and Bioelectronics,* vol. 38, pp. 11-18, 2012.

[77] S. M. U. Ali, H. Z. Ibupoto, S. Salman *et al.*, "Selective determination of urea using urease immobilized on ZnO nanowires," *Sensors and Actuators B,* vol. 160, pp. 637-643, 2011.

[78] Y. Huang, L. Bu, W. Wang *et al.*, "One-pot preparation of uricase-poly(thiophene-2-boronic acid)-Ptnano composites for high-performance amperometric biosensing of uric acid," *Sensors and Actuators B,* vol. 177, pp. 116-123, 2013.

[79] M. Moraes, U. Filho, O. Oliveira *et al.*, "Immobilization of uricase in layer-by-layer films used in amperometric biosensors for uric acid," *J Solid State Electrochem.,* vol. 11, pp. 1489-1495, 2007.

[80] T. Hoshi, H. Saiki, and J. Anzai, "Amperometric uric acid sensors based on polyelectrode multilayer films," *Talanta,* vol. 61, pp. 363-368, 1993.

[81] Y.-C. Luo, J.-S. Do, and C.-C. Liu, "An amperometric uric acid biosensor based on modified Ir-C electrode," *Biosensors and Bioelectronics,* vol. 22, pp. 482-488, 2006.

[82] F. Arslan, "An amperometric biosensor for uric acid determination prepared from uricase immobilized in polyaniline-polypyrrole film," *Sensors,* vol. 8, pp. 5492-5500, 2008.

[83] S. Cete, A. Yasar, and F. Arslan, "An amperometric biosensor for uric acid determination prepared from uricase immobilized in polypyrrole film," *Artificial Cells, Blood Substitutes and Biotechnology,* vol. 34, pp. 367-380, 2006.

[84] Y. Zhang, G. Wen, Y. Zhou *et al.*, "Development and analytical application of an uric acid biosensor using an uricase-immobilized eggshell membrane," *Biosensors and Bioelectronics,* vol. 22, pp. 1791-1797, 2006.

[85] M. Bhambi, G. Sumana, B. D. Malhotra *et al.*, "An amperometric uric acid biosensor based on immobilization of uricase onto polyaniline-multiwalled carbon nanotube composite film," *Artificial Cells, Blood Substitutes, and Biotechnology,* vol. 38, pp. 178-185, 2010.

[86] N. Chauhan, and C. S. Pundir, "An amperometric uric acid biosensor based on multiwalled carbon nanotube-gold nanoparticle composite," *Analytical Biochemistry,* vol. 413, pp. 97-103, 2011.

[87] C. Mateo, J. M. Palomo, G. Fernandez-Lorente *et al.*, "Enzyme and Microbial Technology. Improvement of enzyme activity, stability and selectivity via immobilization techniques," *Enzyme and Microbial Technology,* vol. 40, pp. 1451-1463, 2007.

[88] S. Kwakye, and A. Baeumner, "An embedded system for portable electrochemical detection," *Sensors and Actuators B,* vol. 123, pp. 336-343, 2007.

[89] J. H. Rappole, and A. R. Tipton, "New harness design for attachment of radio transmitters to small passeriness," *J. Field Ornithol.,* vol. 62, no. 3, pp. 335-337, 1991.

[90] K. E. Harr, "Cilinical chemistry of companion avian species: a review," *Veterinary clinical pathology,* vol. 31, pp. 140-151, 2002.

[91] G. S. Wilson, and M. Ammam, "In vivo Biosensors minireview," *The FEBS Journal,* vol. 281, pp. 503-511, 2007.

[92] F. H. Baumann, and R. Baumann, "A comparative study of the respiratory properties of bird blood," *Respiration Physiology,* vol. 31, pp. 333-343, 1977.

[93] R. Prinzinger, A. Prebmar, and E. Schleucher, "Body temperature of birds," *Comp. Biochem. Physiol.,* vol. 99A, pp. 499-506, 1991.

[94] X. Liu, P. Lin, X. Yan *et al.*, "Enzyme-coated single ZnO nanowire FET biosensor for detection of uric acid," *Sensors and Actuators B,* vol. 176, pp. 22-27, 2013.

[95] M. S. Bowlin, and M. Wikelski, "Pointed wings, low wingloading and calm air reduce migratory flight costs in songbirds," *PLoS One,* vol. 3, no. 4, pp. e2154, 2008.

[96] E. S. Bridge, K. Thorup, M. S. Bowlin *et al.*, "Technology on the move: recent and forthcoming innovations for tracking migratory birds," *BioScience,* vol. 61, no. 9, pp. 689-698, 2011.

[97] W. D. Robinson, M. S. Bowlin, I. Bisson *et al.*, "Integrating concepts and technologies to advance the study of bird migration," *Front Ecol Environ,* vol. 8, no. 7, pp. 354-361, 2010.

[98] S. Jenni-Eiermann, L. Jenni, A. Kvist *et al.*, "Fuel use and metabolic response to endurance exercise: a wind tunnel study of a long-distance migrant shorebird," *The Journal of Experimental Biology,* vol. 205, pp. 2453-2460, 2002.

[99] S. Jenni-Eiermann, and L. Jenni, "Metabolic responses to flight and fasting in night-migrating passerines," *J Comp Physiol B,* vol. 161, pp. 465-474, 1991.

[100] R. Schwilch, L. Jenni, and S. Jenni-Eiermann, "Metabolic responses of homing pigeons to flight and subsequent recovery," *J Comp Physiol B,* vol. 166, pp. 77-87, 1996.

[101] A. Gumus, S. Lee, K. Karlsson *et al.*, "Real-time in vivo uric acid biosensor system for biophysical monitoring of birds," *Analyst,* vol. 139, pp. 742-748, 2014.

[102] C. Choleau, J. C. Klein, G. Reach *et al.*, "Calibration of a subcutaneous amperometric glucose sensor implanted for 7 days in diabetic patients Part 2. Superiority of the one-point calibration method," *Biosensors and Bioelectronics,* vol. 17, pp. 641-646, 2002.

[103] L. Jenni, and S. Jenni-Eiermann, “Fuel supply and metabolic constraints in migrating birds,” *Journal of Avian Biology,* vol. 29, pp. 521-528, 1998.

[104] W. H. O. (WHO). "Cholera," Aug 28, 2014.

[105] J. Yadava, M. Jain, and A. Goel, “Detection and confirmation of toxigenic Vibrio cholerae 01 in environmental and clinical samples by a direct cell multiplex PCR,” *Water SA,* vol. 39, no. 5, pp. 611-614, 2013.

[106] M. Maheshwari, K. Nelapati, and B. Kiranmayi, “Vibrio cholerae-A Review,” *Veterinary World,* vol. 4, no. 9, pp. 423-428, 2011.

[107] J. A. K. Hasan, A. Huq, M. L. Tamplin *et al.*, “A Novel Kit for Rapid Detection of Vibrio-Cholerae 01,” *Journal of Clinical Microbiology,* vol. 32, no. 1, pp. 249-252, Jan, 1994.

[108] F. Qadri, J. A. K. Hasan, J. Hossain *et al.*, “Evaluation of the Monoclonal Antibody-Based Kit Bengal Smart for Rapid Detection of Vibrio-Cholerae O139 Synonym Bengal in Stool Samples,” *Journal of Clinical Microbiology*, vol. 33, no. 3, pp. 732-734, Mar, 1995.

[109] H. M. Bolanos, M. T. Acuna, A. M. Serrano *et al.*, “Performance of Cholera-SMART((R)) and Pathogen-Detection-Kit((R)) in the quick diagnosis of cholera,” *Revista Panamericana De Salud Publica-Pan American Journal of Public Health,* vol. 16, no. 4, pp. 233-241, Oct, 2004.

[110] P. Kalluri, A. Naheed, S. Rahman *et al.*, “Evaluation of three rapid diagnostic tests for cholera: does the skill level of the technician matter?,” *Tropical Medicine & International Health,* vol. 11, no. 1, pp. 49-55, Jan, 2006.

[111] P. Mukherjee, S. Ghosh, T. Ramamurthy *et al.*, “Evaluation of a Rapid Immunochromatographic Dipstick Kit for Diagnosis of Cholera Emphasizes Its Outbreak Utility,” *Japanese Journal of Infectious Diseases,* vol. 63, no. 4, pp. 234-238, Jul, 2010.

[112] J. R. Harris, E. C. Cavallaro, A. A. de Nobrega *et al.*, “Field evaluation of Crystal VC (R) Rapid Dipstick test for cholera during a cholera outbreak in

Guinea-Bissau," *Tropical Medicine & International Health*, vol. 14, no. 9, pp. 1117-1121, Sep, 2009.

[113] X. Y. Wang, M. Ansaruzzaman, R. Vaz *et al.*, "Field evaluation of a rapid immunochromatographic dipstick test for the diagnosis of cholera in a high-risk population," *Bmc Infectious Diseases*, vol. 6, Feb, 2006.

[114] A. M. Foudeh, T. F. Didar, T. Veres *et al.*, "Microfluidic designs and techniques using lab-on-a-chip devices for pathogen detection for point-of-care diagnostics," *Lab on a Chip*, vol. 12, no. 18, pp. 3249-3266, 2012.

[115] N. Bunyakul, C. Promptmas, and A. J. Baeumner, "Microfluidic biosensor for cholera toxin detection in fecal samples," *Analytical and bioanalytical chemistry*, pp. 1-10, 2014.

[116] C. D. Chin, V. Linder, and S. K. Sia, "Commercialization of microfluidic point-of-care diagnostic devices," *Lab on a Chip*, vol. 12, no. 12, pp. 2118-2134, 2012.

[117] B. H. Park, Y. T. Kim, J. H. Jung *et al.*, "Integration of sample pretreatment, μPCR, and detection for a total genetic analysis microsystem," *Microchimica Acta*, pp. 1-14, 2013.

[118] F. Ahmad, and S. A. Hashsham, "Miniaturized nucleic acid amplification systems for rapid and point-of-care diagnostics: A review," *Analytica chimica acta*, vol. 733, pp. 1-15, 2012.

[119] M. R. Hartman, R. C. Ruiz, S. Hamada *et al.*, "Point-of-care nucleic acid detection using nanotechnology," *Nanoscale*, vol. 5, no. 21, pp. 10141-10154, 2013.

[120] L. Chen, A. Manz, and P. J. Day, "Total nucleic acid analysis integrated on microfluidic devices," *Lab on a Chip*, vol. 7, no. 11, pp. 1413-1423, 2007.

[121] Q. Wu, W. Jin, C. Zhou *et al.*, "Integrated glass microdevice for nucleic acid purification, loop-mediated isothermal amplification, and online detection," *Analytical chemistry*, vol. 83, no. 9, pp. 3336-3342, 2011.

[122] B. S. Ferguson, S. F. Buchsbaum, T.-T. Wu *et al.*, "Genetic analysis of H1N1 influenza virus from throat swab samples in a microfluidic system for point-of-care diagnostics," *Journal of the American Chemical Society,* vol. 133, no. 23, pp. 9129-9135, 2011.

[123] X. Fang, H. Chen, L. Xu *et al.*, "A portable and integrated nucleic acid amplification microfluidic chip for identifying bacteria," *Lab Chip,* vol. 12, no. 8, pp. 1495-1499, 2012.

[124] L. Jiang, M. Mancuso, Z. Lu *et al.*, "Solar thermal polymerase chain reaction for smartphone-assisted molecular diagnostics," *Scientific reports,* vol. 4, 2014.

[125] M. A. Dineva, L. Mahilum-Tapay, and H. Lee, "Sample preparation: a challenge in the development of point-of-care nucleic acid-based assays for resource-limited settings," *Analyst,* vol. 132, no. 12, pp. 1193-1199, 2007.

[126] S. K. Njoroge, H.-W. Chen, M. A. Witek *et al.*, "Integrated microfluidic systems for DNA analysis," *Microfluidics*, pp. 203-260: Springer, 2011.

[127] R. H. Liu, J. Yang, R. Lenigk *et al.*, "Self-contained, fully integrated biochip for sample preparation, polymerase chain reaction amplification, and DNA microarray detection," *Analytical chemistry,* vol. 76, no. 7, pp. 1824-1831, 2004.

[128] C.-Y. Lee, G.-B. Lee, J.-L. Lin *et al.*, "Integrated microfluidic systems for cell lysis, mixing/pumping and DNA amplification," *Journal of Micromechanics and Microengineering,* vol. 15, no. 6, pp. 1215, 2005.

[129] L. A. Marshall, L. L. Wu, S. Babikian *et al.*, "Integrated printed circuit board device for cell lysis and nucleic acid extraction," *Analytical chemistry,* vol. 84, no. 21, pp. 9640-9645, 2012.

[130] C. Schrader, A. Schielke, L. Ellerbroek *et al.*, "PCR inhibitors–occurrence, properties and removal," *Journal of applied microbiology,* vol. 113, no. 5, pp. 1014-1026, 2012.